12

ON-CHIP INTEGRATION OF FUNCTIONAL HYBRID MATERIALS AND COMPONENTS IN NANOPHOTONICS AND OPTOELECTRONICS

Talha Erdem and Hilmi Volkan Demir

Bilkent University, Ankara, Turkey

Incorporation of custom-designed nanomaterial into nanophotonic devices and components in optoelectronic systems enables the realization of optical functionalities favorably controlled with external optical and electrical effects. To this end, innovative nanophotonic devices and optoelectronic systems are developed using multiple combinations of nanostructures (epitaxially grown, chemically synthesized, deposited, plated, etc.) that are embedded in hybrid architectures and on-chip integration of components for a variety of applications including light generation, displays, modulation, sensing, imaging, and communications in a wide spectral range from ultraviolet (UV) to visible to infrared.

Such integration of functional materials and components in optoelectronics requires the use of different methods developed for chip-scale integration at the range of micrometers to nanometers, including monolithic integration, hybrid integration, layer-by-layer assembly, and directed assemblies (electrical, optical, mechanical, etc.). This chapter reviews these state-of-the-art integration approaches currently used in optoelectronics.

Ceramic Integration and Joining Technologies: From Macro to Nanoscale, First Edition.
Edited by Mrityunjay Singh, Tatsuki Ohji, Rajiv Asthana, Sanjay Mathur.
© 2011 The American Ceramic Society. Published 2011 by John Wiley & Sons, Inc.

Additionally, the chapter summarizes those innovative integration approaches that are presently being investigated for cutting-edge optoelectronics and nanophotonics.

MONOLITHIC INTEGRATION TECHNIQUES

Optoelectronic components used in current communication systems are typically based on discrete components. These components with different functions are generally combined with each other using fiber splices to provide a specified function. Although the approach of packaging each component individually and then connecting them through fiber connections is a common practice, it manifests some disadvantages. One of them is the great difficulty in efficiently coupling light to and from each discrete chip, which is one of the main sources of optical loss at the system level. In addition, this approach also places a burden at the system implementation level due to cost issues.

To address these problems, monolithic integration may provide possible solutions [1]. For example, using the on-chip integration method, device-to-device coupling problem can be completely eliminated, conveniently leading to a significant decrease in packaging costs and sizes. Additionally, elimination of possible mechanical movements in the structure and possible reduction of driving currents may reduce the power consumption of such integrated chips and may increase the reliability of the full system.

For monolithic integration to become useful and meaningful, a list of some requirements should be fulfilled [2]:

1. The operation of one component should not be affected by the operation of the other components. In other words, each component should function as if it is discrete.
2. Trade-off between fabrication difficulty and performance optimization should be carefully considered because a careless design may increase the overall cost and/or may decrease the device performance.
3. The integration method should not be costly and time-consuming. There are several monolithic integration schemes.

Butt Joint Growth

Butt joint growth is based on the removal of a specific part of the epitaxial region (e.g., waveguide/multiple quantum well [MQW] region and, subsequently, the nonplanar selective regrowth to fill in the removed part (e.g., with desired band edge and waveguide architecture). The main advantage of this integration technique is its high versatility [3]. An exemplary cross-section of butt joint grown epitaxy is shown in Figure 12.1a. In this case, for example, for a laser diode, the flexibility of this process comes from the possibility to grow a quantum well active region for a maximized modal gain. Also, allowing each growth to lead to a desired absorption band edge is an additional strength of this approach. In spite of the ability to separately optimize individual components on the chip [4], there is also some difficulty that arises with the requirement to match the growth thicknesses and to achieve the desired composition to avoid reflection and

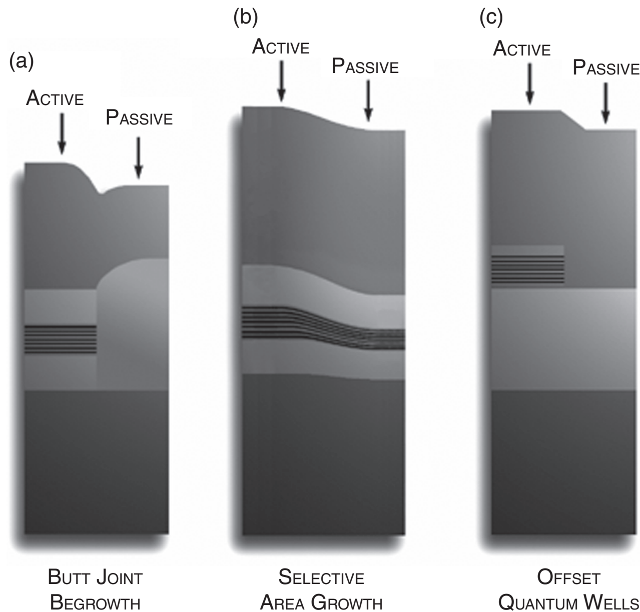

Figure 12.1. (a) Butt joint growth, (b) selective area growth, and (c) offset quantum well techniques showing cross-sectional active and passive sections perpendicular to the growth direction [4].

loss at the interfaces [3]. Increasing the number of desired band edges and waveguide architectures increases the complexity since each new band edge and structure requires an additional regrowth [4].

Selective Area Growth (SAG)

The SAG technique can be used effectively to provide multiple band edges across the epitaxial wafer in a single growth step [5]. This method involves patterning of a dielectric mask on the epiwafer, which is followed by the epitaxial growth (e.g., metal organic chemical vapor deposition [MOCVD] growth). This dielectric mask limits the growth. After butt joint growth, additional regrowth for the upper cladding is performed following the removal of the dielectric mask (Fig. 12.1b). For example, in the case of making a waveguide that integrates a laser diode with a modulator diode along the length of the waveguide, the centered multiple quantum well (c-MQW) active regions in the waveguide are grown on a single chip both for maximum gain in the laser diode section and for maximum electroabsorption in the quantum well electroabsorption modulator (QW EAM). As this technique is based on the contrast in the surface kinetics of the growth elements on the semiconductor and dielectric, the reactor conditions should be controlled very carefully. However, one problem is that the surface diffusion around the transition region might be on the order of tens of micrometers. Also, thickness variation may cause a nonideal optical mode overlap with the MQW region [4].

Offset Quantum Wells

This method involves the growth of the MQW active region on a passive bulk waveguide. This technique allows the nonabsorbing waveguide section to be left for the selective etching of MQWs because the gain is not a concern in these etched regions. After building the active and passive regions, the upper cladding is regrown in this technique as well (Fig. 12.1c) [6]. The strength of this technique lies in its simplicity. However, allowing only for two band edges at most (one from MQW and one from the waveguide) is a drawback of this method [4].

The offset quantum well method can be improved with the addition of a wider band gap quantum well in the passive waveguide [6], known as dual offset quantum wells, shown in Figure 12.2a. This improvement provides more efficient electroabsorption and phase modulators by using a quantum-confined Stark effect resulting in a more abrupt absorption edge [2].

Quantum Well Intermixing (QWI)

Another method for the monolithic integration is the QWI technique. In this method, the metastable nature of gradient at the interfaces is used. Diffusion tendency under compositional/concentrational gradients is the driving force of this process. The diffusion rate can be adjusted/increased using catalysts. QWI process can be made selective by using a lithographically defined catalyst patterning. Some of the techniques used for

Figure 12.2. Schematics for (a) dual quantum wells and (b) quantum well intermixing methods [4].

QWI are impurity-induced disordering (IID) [7], impurity-free vacancy-enhanced disordering (IFVD) [8], photoabsorption-induced disordering (PAID) [9], and implantation-enhanced interdiffusion [10]. A schematic representation of the process is given in Figure 12.2b. QWI does not change the average composition; however, it changes the compositional profile slightly. Therefore, reasonable index continuity is observed at the interface between adjacent parts. This property of the QWI method avoids parasitic reflections, which would otherwise decrease the performance of the device [4].

Coldren and coworkers used the implant-enhanced interdiffusion technique to build up a 10-Gb/s widely tunable transmitter. This technique involves the diffusion of point defects created during ion implantation into an InP implant buffer layer grown on an MQW active region [2]. Good spatial resolution and controllability (using annealing time, temperature, and implant dose) are the strengths of this method [11].

The IID method relies on the use of impurities, generally dopants, to change the equilibrium defect concentration, which depends on the Fermi level to enhance self-diffusion into the crystal resulting from intermixing [7]. A disadvantage of this method is the adverse effects of dopants on the electrical properties of the device [12].

The PAID technique is based on the heating of the MQW structure through laser irradiation to provide intermixing [12]. The drawback of this technique is its poor spatial resolution, although the material quality is very high [9].

The IFVD method relies on the postgrowth introduction of vacancies that diffuse through the lattice while exchanging places with adjacent atoms as a result of a thermal process. This diffusion mechanism is the driving force of the intermixing for this technique. In spite of its advantage of simplicity, high annealing temperatures to adjust the quantum well are a disadvantage of this method [9].

Multigrowth Monolithic Integration

Sabnis et al. proposed and demonstrated an improved version of multistep selective area growth (MSAG) monolithic integration technique [13]. This approach mainly consists of five steps:

1. Proper MSAG surface preparation and device isolation are maintained by stopping the incorporation of buried epitaxial etch. Thanks to these layers, it is possible to integrate different epitaxial layers with clean and planar surfaces before epitaxial regrowths. Sequential surface preparation for MSAG can be realized by burying multiple etch-stop layers, one for every MSAG process.
2. Different epitaxial structures are combined by an MSAG process.
3. Device mesas in the SAG are constructed by an MSAG epitaxy etching while using selective wet etches and shallow dry etches.
4. Planarization and passivation processes are applied.
5. Another planarization and passivation process is applied to enable multilevel metal routing for maintaining the desired circuit architecture. After the wafer planarization, interconnection of metal from level to level is still needed. This requirement is fulfilled by using vias and plug metallization. Another approach

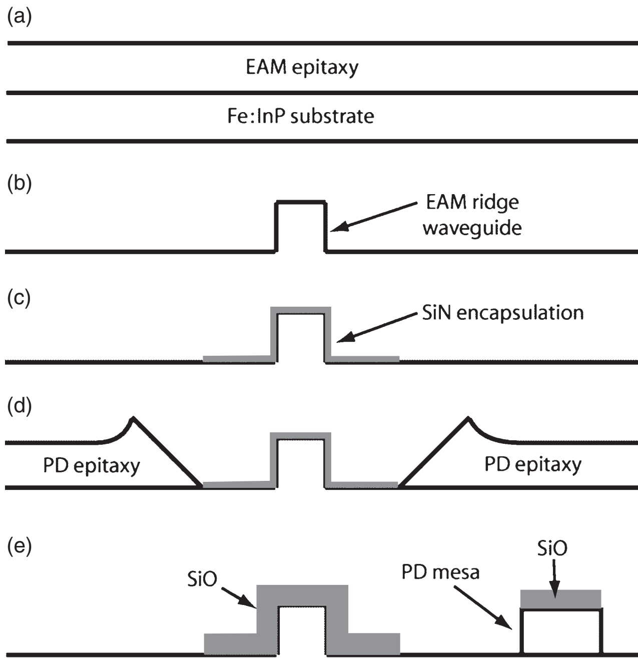

Figure 12.3. MSAG process for the monolithic integration of a photodetector (PD) and an electroabsorption modulator (EAM): (a) epitaxial growth of EAM, (b) ridge etching of EAM, (c) SiN mask definition for SAG, (d) PD SAG, and (e) PD mesa etch [13].

is to etch the planarization material such that a slope is constructed at the interface between layers where the metal connection is desired.

These steps are shown in Figure 12.3.

Surface Passivation and Planarization

During the selective removal of the epitaxially grown material by vertical etching, the sidewalls of the device are typically left exposed. These regions are chemically active and may introduce surface states, which further results in current leakage and stability problems. Sidewall passivation and planarization of the passivation material are therefore required procedures for the vertically etched III–V semiconductor devices [14]. The sidewall passivation suppresses the leakage current, whereas the planarization of the passivation material is needed for the metal interconnection and device integration.

In the etch-back planarization method [15], which is a conventional approach, the planarization of the entire wafer is difficult to seal and passivate device sidewalls. To solve this problem, Demir et al. proposed an approach to realize self-aligning planarization and passivation. In this method, the passivation is achieved by the use of a passivation polymer to passivate the sidewalls across the epitaxial wafer.

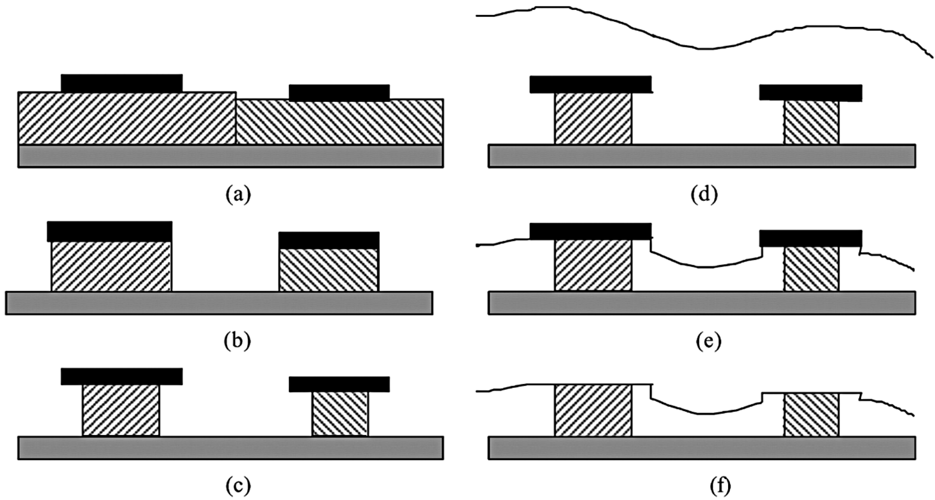

Figure 12.4. Illustration of self-planarizing passivation sequence: (a) The hard mask on the epitaxial wafer is defined; (b) device areas are patterned by vertical etching; (c) the device materials underlying the hard mask perimeters are removed for the undercut creation; (d) the device areas are sealed; (e) the cured polymer is etched back; and (f) the hard mask is removed [14].

The process can be summarized in Figure 12.4 as follows: (1) A dielectric mask is defined on the wafer, which is maintained in the subsequent steps; (2) by vertically etching the unmasked parts of the wafer, the semiconductor device area, which is masked, is defined; (3) the sidewalls of the semiconductor mesa are selectively etched horizontally to form an undercut beneath the hard mask to protect the device as a roof; (4) the sidewalls of the device layers under the hard mask are sealed and passivated with a spin-on polymer; (5) the cured polymer past the top level of the hard mask is etched back with an anisotropic dry etch; and (6) the hard mask is removed in order to construct a passivation structure with the polymer around the device perimeter. In this work, benzocyclobutene (BCB) is used as the passivation polymer, while silicon nitride or silicon oxide is used as the hard mask [16].

Via and Trench Building for Metal Contacts

In III–V semiconductor materials, vias and trenches are used for metal contacting [17]. In the work of Zheng et al., the construction of these structures involves the use of a sacrificial layer, which is made of either a SiO_2 dielectric hard mask layer on the device layers or a semiconductor layer grown onto the device epitaxial layer, both before patterning. The construction steps follow: (1) formation of a hard mask using conventional dielectric thin-film deposition, (2) etching of the semiconductor by reactive ion etching using the hard mask, (3) spinning of a polymer layer and back etching within the hard mask for every device in the wafer, and (4) removal of the hard mask by wet etching to have a via structure. This procedure is illustrated in Figure 12.5.

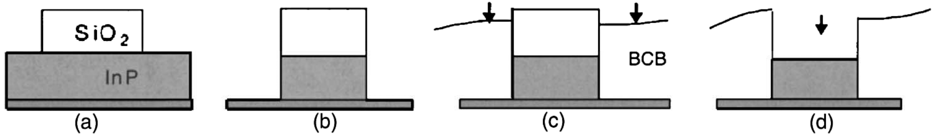

Figure 12.5. Schematic illustration of via and trench formation: (a) formation of the hard mask, (b) etching the semiconductor to define the active region, (c) spinning and back etching of the polymer, and (d) removal of the hard mask to obtain via and trench opening [17].

NANOFABRICATION TECHNIQUES

Nanoscale material design and nanoscale fabrication techniques are in general grouped as top-down and bottom-up approaches [18]. The top-down method involves various techniques of lithography to pattern nanoscale structures. This approach may make use of serial and parallel techniques to pattern features. On the other hand, the bottom-up method is based on the interactions between molecules and colloidal particles to construct discrete nanoscale structures in two and three dimensions.

Photolithography and scanning beam lithography are considered in the conventional top-down approach. Their limitations are their high costs, difficulty in accessing the required facilities, and lack of applicability in a wide range of problems. Less conventional approaches also cover both top-down and bottom-up methods. Molding, embossing, and printing can be classified as top-down methods; on the other hand, scanning probe lithography (SPL), edge lithography, and self-assembly can be interpreted as bridge methods between the top-down and bottom-up approaches.

In general, conventional techniques suffer high cost and low throughput, and they are typically restricted to planar fabrication in semiconductor materials and are incompatible with many problems in nonstandard fabrication. Additionally, these techniques expose substrates to corrosive etchants, cause high-energy radiation, and require high temperatures. These are the driving force for the investigation of new nanofabrication methods.

Photolithography

Photolithography is the chosen method for the manufacturing of microelectronic devices by the industry. In photolithographic systems, mask aligners shine collimated light trough a quartz plate that supports a patterned chromium coating and expose a photoresist thin film coated on a planar substrate. The photoresist is an organic material that becomes insoluble or more soluble as a result of chemical changes when exposed to high-energy (short wavelength) light [19–21]. The photoresist exposed to light is soaked in a solvent that dissolves exposed or unexposed regions. This process thus allows for transferring the pattern of the starting mask to the exposed and developed photoresist film on the substrate. This patterning also functions as a mask for the substrate during subsequent steps (Fig. 12.6). A modern photolithography system can pattern with a resolution of 27 nm [22]. In 2005 semiconductor nanofabrication productions, photolithography is used

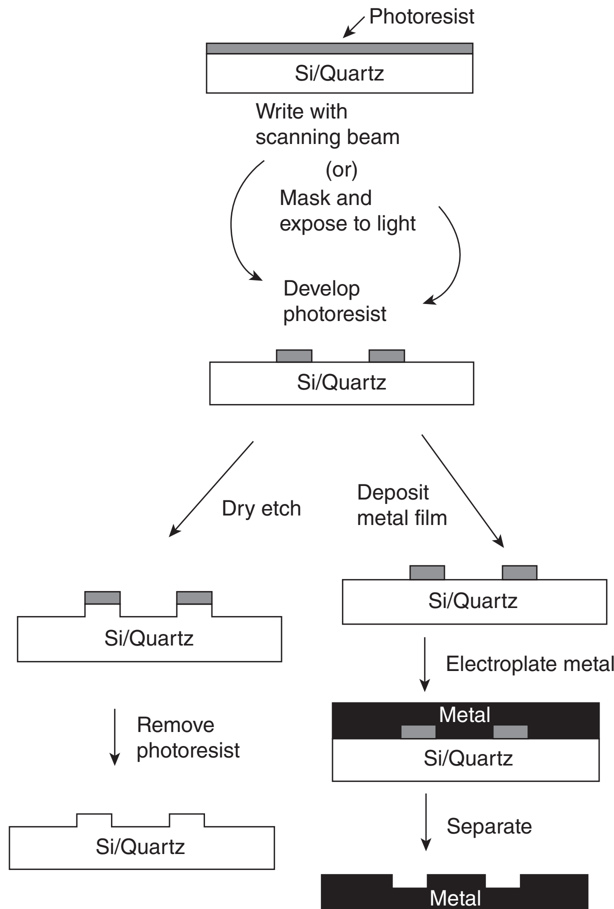

Figure 12.6. Schematic illustration of fabrication using photolithography and electroplating in hard materials [18].

to pattern 37-nm-wide features with 193-nm wavelength light. Attempts to decrease these sizes require optical proximity correction (OPC) and phase-shift mask technology; however, all of these modifications increase the cost significantly.

Immersion lithography is proposed as a potential lithography method for features with sub-50-nm resolution exposing light at 193 nm [23]. This lithography technique is the analogous of immersion microscopy that is widely used in biology [24]. In this technology, the imaging resolution is improved by the increased refractive index of the medium between the imaging lens and the imaging plane [24]. This method requires contacting the photoresist-coated substrate and mask with water (or another solvent) and using complex, aspheric, catadioptric lenses. Another solution toward patterning smaller structures using photolithography might be decreasing the wavelength of exposing light. This, however, requires new types of photoresists, new light sources, and new types of optics.

The main drawback of the photolithography lies on the time and cost requirements to fabricate the photomask. On the other hand, interferometric lithography provides the production of simple patterns without using a photomask [25, 26]. This method is based on the constructive and destructive interference of multiple laser beams at the surface of photoresist. Although no photomask is needed for this method, pattern projection is restricted only for regularly spaced arrays.

Scanning Beam Lithography

Scanning beam lithography is a process that is often used for the production of photomasks for projection lithography instead of actual device fabrication. Patterning dense arrays of sub-20-nm features on an area of 1 cm^2 takes ca. 24 h [18]. Therefore, scanning beam lithography is restricted to small areas or to areas with low densities.

Scanning beam lithography is a slow process compared to photolithography. However, this technique also allows for the fabrication of arbitrary patterns. Scanning beam lithography has three classes: (1) scanned laser beams with ca. 250-nm resolution (the least expensive), (2) focused electron beams with sub-50-nm resolution, and (3) focused ion beam (FIB) lithography systems with sub-50-nm resolution (often used in research).

High-resolution patterning comes with some trade-offs. An increase in the resolution can be achieved only by decreasing the diameter of the particle beam. As a result, the beam current also decreases, which results in an increased processing time, required to pattern the entire surface.

An FIB enables writing patterns into a photoresist or directly onto the substrate [27]. Using this technique, materials can be selectively removed through ion bombardment, or patterns can be created additively by localized chemical vapor deposition or by ion deposition [28–30]. FIB lithography enables patterning features in a semiconductor with resolution down to 20 nm and with lateral dimensions down to 5 nm [31].

SPL

SPL is a promising tool for manipulation and imagination with an atomic-scale resolution [32]. However, this tool requires improvements for use in large-area manufacturing. Scanning tunneling microscopy (STM) (Fig. 12.7A), atomic force microscopy (AFM), and near-field scanning optical microscopy (NSOM) are some of the most important SPL techniques. Although atomic-scale manipulations on surfaces are possible using these techniques, there is still a long way to go in order to make these techniques practical [18]. In general, the operation of SPL can be described as the localized modification of surface by oxidation or by material transfer using a sharp probe in contact with the surface [18, 33, 34].

Serial Patterning of Surfaces

Dip-pen nanolithography (DPN) provides methods to dispose nanoparticles or other molecules selectively onto a surface [34]. Inking AFM tips with a solution of the materials to be transferred enables positioning the material onto the substrate when the

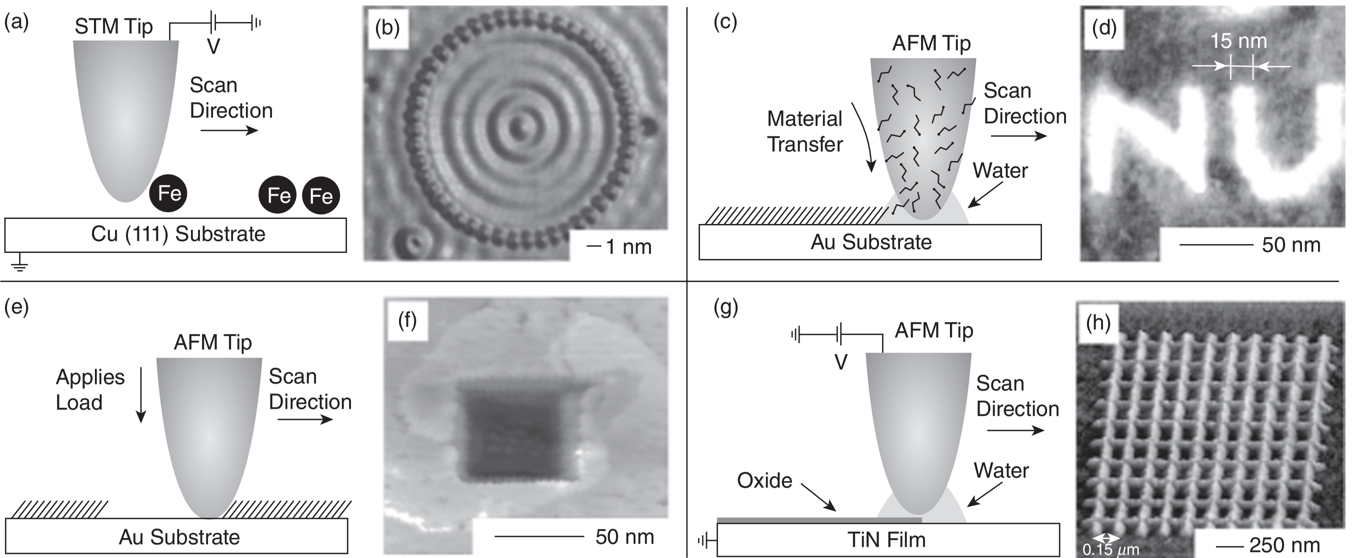

Figure 12.7. Schematic illustrations of four approaches to SPL and patterns produced using (A) STM [35] (B) to make a quantum corral of a 48-atom Fe ring formed on Cu enclosing a defect-free region [198]; (C) dip-pen lithography (DPN) [35] (D) to pattern features down to 15 nm [199]; (E) nanoshaving [35] to remove regions of SAMs (F) to pattern a square hole within octadecane thiolate SAMs on Au [200], and (G) scanning electrochemical oxidation [35] to selectively oxidize a surface (H) to build ca. 50-nm-wide lines of oxide written on TiN [38].

probe scans the surface (Fig. 12.7C) [35]. Using DPN 15-nm patterns is achievable (Fig. 12.7D). This mechanism cannot be understood perfectly; however, several theories have been proposed. According to one theory, a water layer between the tip and surface makes the material transfer possible. According to another one, the material transfer is possible due to the solid–solid interactions. Humidity, chemical interaction with the substrate, radius of curvature of the probe, and linear velocity of the probe determine the spreading of the ink.

Another approach for the patterning of the surfaces is the selective removal of material from the surface. This removal operation is performed by mechanical abrasion using a scanned AFM probe [36]. The probe displaces a thin film when the contact load between the tip and the substrate is higher than the displacement threshold of the surface layer. This process is called "nanoshaving," and it is used for the patterned removal of the self-assembled monolayers (SAMs) (Fig. 12.7E, F) [20]. Material abrasion can also be performed after multiple scans when the contact load of the AFM tip is still below the displacement threshold of the material [37]. Nonuniformities in the topography, however, can cause irregular patterns. A surface can be chemically modified using SPL. This operation can be made using a conductive AFM or STM tip. In Figure 12.7G, H, a TiN substrate patterned by localized electric field-induced oxidation using a conductive AFM probe is shown [38].

Parallel Patterning of Surfaces

Although SPL methods provide flexible patterning possibilities, the use of a single tip makes these methods impractical for mass production. Using multiple probes that work in parallel may remedy this problem [35, 39]. A two-dimensional array of independently addressed AFM probe is developed, and this concept is known as "millipede" (Fig. 12.8) [39]. In this approach, deflection in the vertical direction and resistive heating can also be provided.

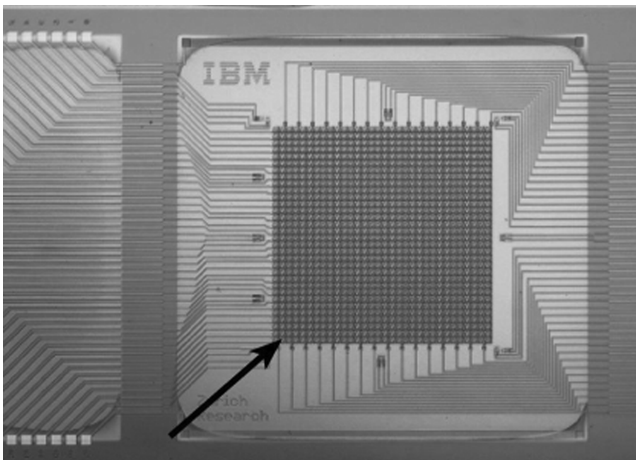

Figure 12.8. Millipede approach example [39].

Edge Lithography

In edge lithography, topographic edges are used in the fabrication of nanoscale structures [35, 40, 41]. By using this method, arrays of structures that are smaller than 100 nm can be produced. Edge lithography can be grouped in two techniques: (1) edge lithography using topography-directed pattern transfer and (2) cleaved or cut edge nanostructures.

Pattern Transfer Directed by Topography. Decoration of step edges: At the step edges of single-crystalline surfaces, metals and other materials are deposited selectively with success [42, 43]. This deposition procedure results in the generation of continuous nanowires.

Electrodeposition or etching at the edge defined defects in SAMs: Selective removal and deposition of materials are the other ways of patterning nanostructures. [40, 44, 45] An example might be that sharp metal corners within topographically patterned metal substrates avoiding well-ordered SAM formation expose underlying metal at the edges (Fig. 12.9A) [45]. Selective etching of this metal makes it possible to transfer the outline of the patterned metallic topography onto the underlying film.

For example, SAMs can be formed on silver, but not on titanium, when the patterned substrate is put into an alkanethiol solution. The exposed Ti/TiO_2 layer builds a ~5-nm gap in the SAM. This gap may serve as a nanoelectrode upon which metal can be electrochemically deposited (Fig. 12.9B) [31]. A curved or flat substrate can be produced while using an adhesive to remove these structures. Incident light can be polarized using the arrays of Cu lines on an adhesive (Fig. 12.9C) [45].

Controlling undercutting at edges: After the deposition of a thin film, topographic features can be undercut in a controlled fashion. This technique also provides the fabrication of nanostructures (Fig. 12.9D) [44]. For example, isotropic wet etching of a thin metal film on a silicon or CaF_2 substrate covered with a photoresist provides patterned structures following the undercutting of the photoresist [44]. Trenches at the edges of the pattern can be observed by lifting off the photoresist (Fig. 12.9E, F) [44].

Phase-shifting photolithography: Controlling the phase of the exposing light, which is used to create narrow constructive and destructive interference, allows for significant modifications in the intensity profile when the light meets the vertical edges of a transparent, topographically patterned substrate. This phenomenon is used to create dark and bright spots of incident light onto the photoresist. Optimally, the light should have a phase shift of π at the photoresist–mask interface.

Cleaved or Cut Edge Nanostructures. Various techniques to grow thin films with a careful control of thickness between 1 and 50 nm enable additional following methods for the fabrication of nanostructures.

Edges Produced by Fracture. Simple quantum structures can be patterned using the cross-sections of multilayer films produced by molecular beam epitaxy (MBE) as templates [41]. For example, field-effect transistors (FETs) with a 20-nm gate length are produced using this procedure. In this example, alternating

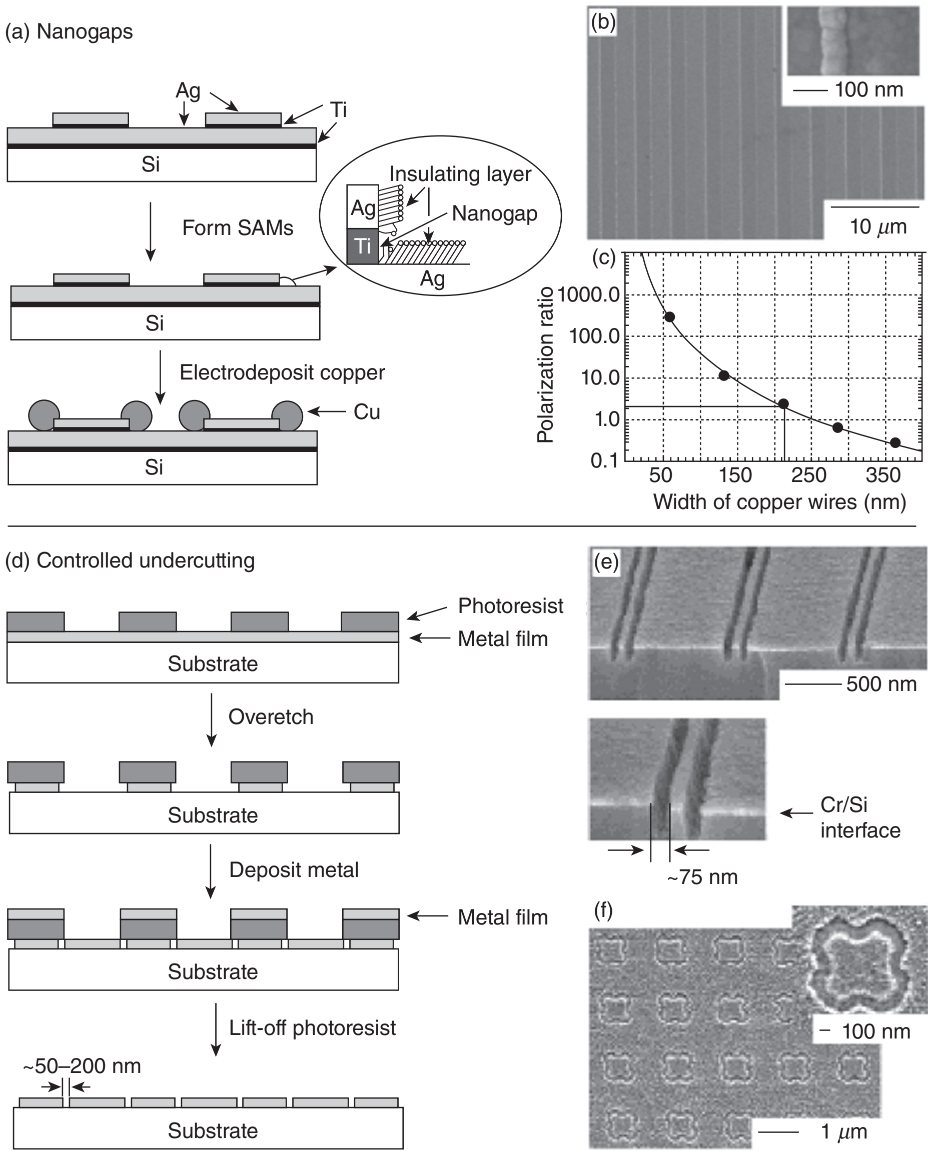

Figure 12.9. (A) Production of nanogaps by engineering defects in Ag SAMs, (B) scanning electron microscope (SEM) image of 70-nm-wide lines of Cu selectively electrodeposited on these nanogaps [45], (C) polarization ratio of the electric component of light as a function of line width [45], (D) illustration of controlling undercutting, (E) cross-section of ~75-nm-wide trenches in silicon [44], and (F) frequency-selective surface of 100-nm-wide trenches in Al [44].

layers of AlGaAs and GaAs, which are grown using MBE, are used (Fig. 12.10A, B) [41]. Parallel arrays of nanowires can be built using selectively etched, multilayered MBE-grown GaAs/AlGaAs substrates as the physical templates with narrowly spaced groves for patterning by physical vapor deposition (PVD). The widths of the wires are determined by the GaAs layers, and the spacing between wires is controlled by AlGaAs layers [46].

Edges Produced by Sectioning with a Microtome. A nanostructured edge can be built up by embedding a thin film in a matrix and by taking its cross-section. One approach to do this is based on removing the matrix material by repeated sliding against a rough surface [47, 48]. This technique can be extended using a microtome to section a polymer-encapsulated patterned metal film (Fig. 12.10C, D) [49, 50].

Edges Positioned by Reorientation. Tipping periodic arrays of posts onto one side can be used to pattern large-scaled areas (~cm^2) (Fig. 12.10E) [51]. This process enables one to generate regular arrays of features in nanoscale lateral dimensions in plane (Fig. 12.10F, G).

Soft Lithography

Soft lithography is a collection of techniques that involve organic (soft) materials to provide replication and pattern transfer on a wide range of length scales (from nanometer to centimeter) [41]. The term soft is used for the stamp and/or substrate composed of materials including polymers or SAMs. The pattern transfer is achieved generally by first fabricating a topographical patterned master then molding this master to build up a patterned stamp, and finally generating a replica of the original template (Fig. 12.11). Conventional methods are good enough for the fabrication of masters, whereas the rest of the process needs new techniques. Soft lithography can be described in three steps: replica molding, embossing, and microcontact printing.

Replica Molding. Replica molding transfers topographical features from a rigid or elastomeric mold into another material by solidifying a liquid in contact with the original pattern [52]. Step-and-flash lithography technique (Fig. 12.12A), developed by Willson and colleagues, involves the use of a transparent master, for example, quartz [53]. After contacting this mold with a low-viscosity, photocurable polymer, the polymer is held under UV light. With this method, features as small as 30 nm can be produced [54]. The strengths of this approach are the rapid cyclic time (<5 min/replication) and the ability of optical mold alignment with features on the underlying surface [53, 55]. However, the difficulty of patterning nanostructures on nonplanar surfaces replicating isolated features caused by air at the mold–polymer interface is the weakness of this technique. Replica molding can also be achieved using deformable templates, for example, polydimethlysiloxane (PDMS). Figure 12.12B makes an illustrative summary of this procedure. Another way for the replica molding is the microtransfer molding, in which the liquid prepolymer is put into the molding regions. After cleaning the excess polymer using a flat edge (a doctor blade), the mold is placed in contact with the rigid substrate. Finally, the prepolymer is cured (Fig. 12.12C). This technique is used for

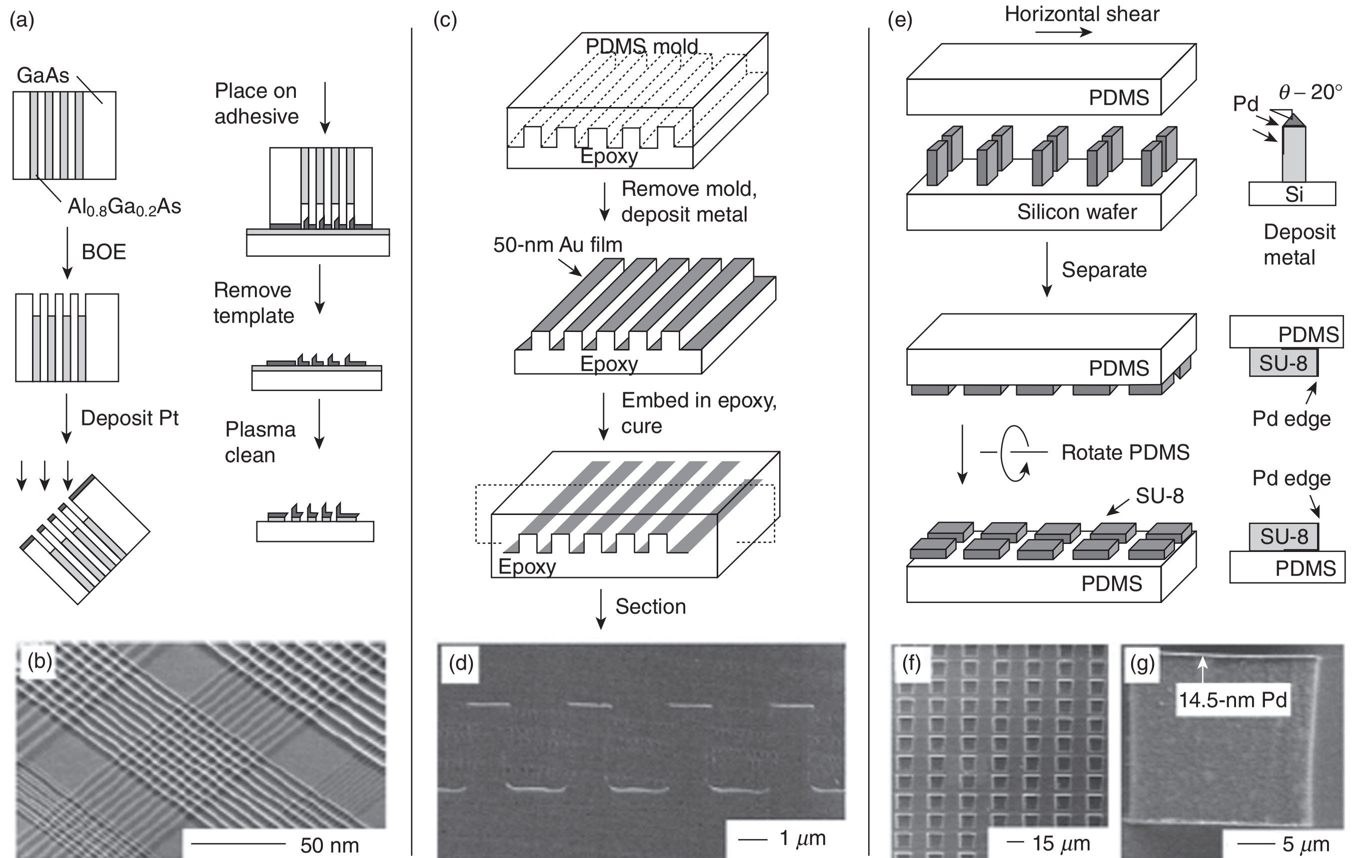

Figure 12.10. (A) A schematic illustration and (B) SEM images of Pt nanowire arrays [41], (C) illustration of the fabrication of a patterned array of epoxy-embedded conducting metal edges, (D) SEM image of these metal edges [41], (E) schematic illustration of microdomino array uniformly collapsed after the application of a horizontal shear (PDMS) [42], (F) SEM images of these structures, and (G) a ~15-nm-wide edge of Pd on a collapsed post [42]. BOE, buffered oxide etch.

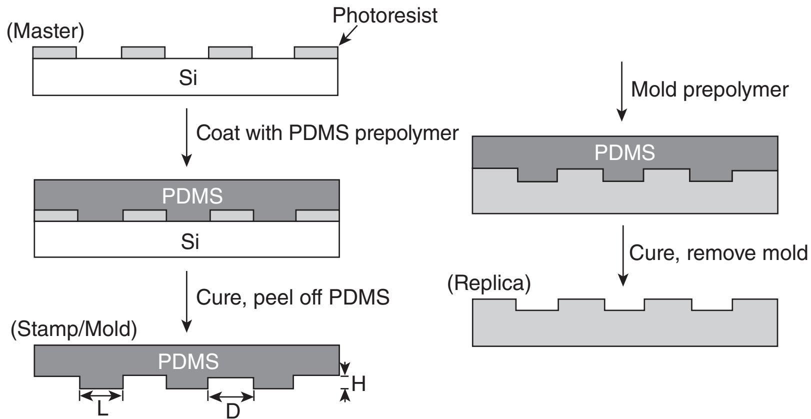

Figure 12.11. Schematic illustration of soft lithography [35].

Figure 12.12. Schematic illustrations of molding techniques: (A) step and flash, (B) replica molding (RM), (C) microtransfer molding (μTM), and (D) micromolding in capillaries (MIMIC) [35].

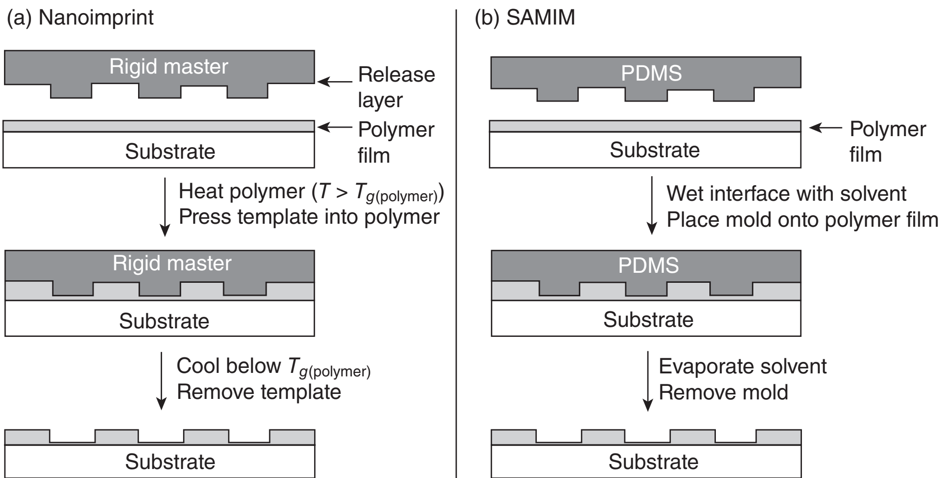

Figure 12.13. Illustration of embossing procedures: (A) nanoimprint lithography and (B) solvent-assisted micromolding (SAMIM) [35].

patterning planar or curved surfaces [56]. Micromolding in capillaries is also another way of molding [57]. This technique involves the use of capillaries to fill the channels of a topographically patterned stamp with a liquid. The precursor material is cured within the capillaries and the mold is removed (Fig. 12.12D).

Embossing and Nanoimprinting. Embossing techniques are used for manufacturing compact disks and digital versatile disks (DVDs). The modifications of these techniques can also be extended to nanofabrication with a resolution below 50 nm [58]. Nanoimprint lithography is used to transfer a pattern from a rigid mold into a deformable material coated on a rigid surface (Fig. 12.13A). In general, the material is first heated under pressure. The mold is later removed after cooling the material below its glass transition temperature. A structure that is as small as 10 nm can be replicated using imprinting with aspect ratios 10:1 [59]. In this technique, rigid mold and spin-cast polymer film must be positioned in parallel, and the applied pressure should be uniform. These are the main drawbacks of this approach.

Embossing can also be applied using soft mold. Using PDMS mold solvent-assisted micromolding (SAMIM) takes place with an appropriate solvent instead of using rigid mold, high temperatures, or pressures (Fig. 12.13B). After placing the polymer into the mold, evaporation is completed and, finally, the mold is removed.

Microcontact Printing. The general procedure for microcontact printing involves contacting the surface of a metal, metaloxide, or semiconductor with a topographically patterned PDMS stamp, wetted with a solution of an alkanethiol or other molecules that can form SAMs for a few seconds. An ordered monolayer is rapidly formed at the points of contact. The strengths of microcontact imprinting for fabricating nanoscale structures are that the minimum feature size on the pattern depends on the physical

dimensions of the step (instead of optical diffraction), that the stamp provides mechanical flexibility, and that various types of materials can be used as inks on different materials. Blurring of pattern by lateral diffusion of the ink, the deformation in the pattern reflecting deformations in the stamp, and high number of defects in the film are, on the other hand, the disadvantages of this technique [60].

GENERAL SELF-ASSEMBLY TECHNIQUES

Self-assembly is defined as the self-organization of different components into regular structures without human intervention. Self-assembly processes can be observed and used in various fields of technology and nature. For nanotechnology, self-assembly appears to be one of the fundamental and most promising techniques to construct nanostructures. Self-assembly can be classified mainly into two groups: static self-assembly and dynamic self-assembly.

Static self-assembly is based on the systems that are in equilibrium and that do not dissipate energy (Fig. 12.14) [61]. Molecular crystals and globular proteins are among the examples [62, 63]. Structures formed by static self-assembly may require energy during their building process; however, once they are formed, the structure is stable and therefore no energy is further needed to hold the system stable. Most of the research projects focus on this type of self-assembly.

In self-assembly, the components should be able to change their positions with respect to each other so that they can balance attractive and repulsive forces in their steady-state position. In molecular scale, these forces are often observed as the results of van der Waals, electrostatic, hydrophobic, and hydrophilic interactions. The forces observed in the self-assembly of larger structures include gravitational force, external electromagnetic forces, and magnetic, capillary, and entropic forces. Since the movement of particles is critical for the self-assembly processes, the interactions occur often in liquid media or on smooth surfaces.

Although researches are mainly focused on static self-assembly, dynamic self-assembly also has a significant importance (Fig. 12.15) [60]. The main essence of dynamic self-assembly is to mimic the reactions and structures that enable the continuity of life in nature. In living cells, many self-assembly processes are dynamic. When the energy flow stops, these cells die, showing the importance of these processes.

Dynamic self-assembly can also be observed in nonliving environments and systems. Oscillating reactions in solution and on the surface of catalysts, Rayleigh–Bernard convection cells are some examples for dynamic self-assembly.

Templated Self-Assembly

Templating self-assembly makes the creation of patterns into a self-assembled structure possible [20]. Additionally, it is used for increasing the order of the self-assembled structure. Surface topography, electric and magnetic fields, or shear forces can be used to direct self-assembly. Top-down methods to direct the bottom-up assembly of molecules and other particles are often preferred in the templated self-assembly approach [64].

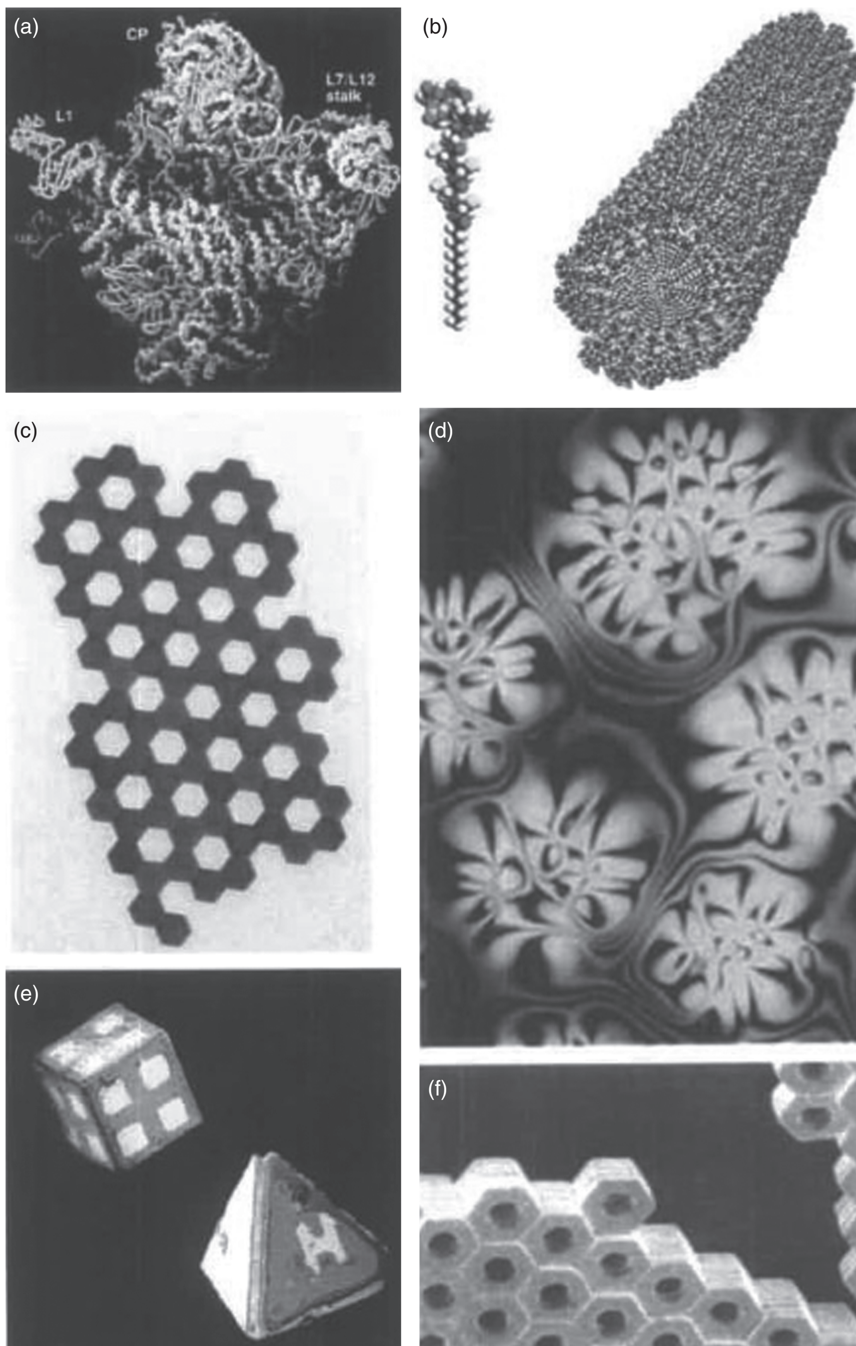

Figure 12.14. Examples of static self-assembly: (A) crystal structure of a ribosome [201], (B) self-assembled peptide-amphiphile nanofibers [95], (C) an array of millimeter-sized polymeric plates [61], (D) thin film of a nematic liquid crystal on an isotropic substrate [61], (E) micrometer-sized metallic polyhedra folded from planar substrates [202], and (F) a three-dimensional aggregate of micrometer plates [203]. (D) Courtesy of O. Lavrentovich.

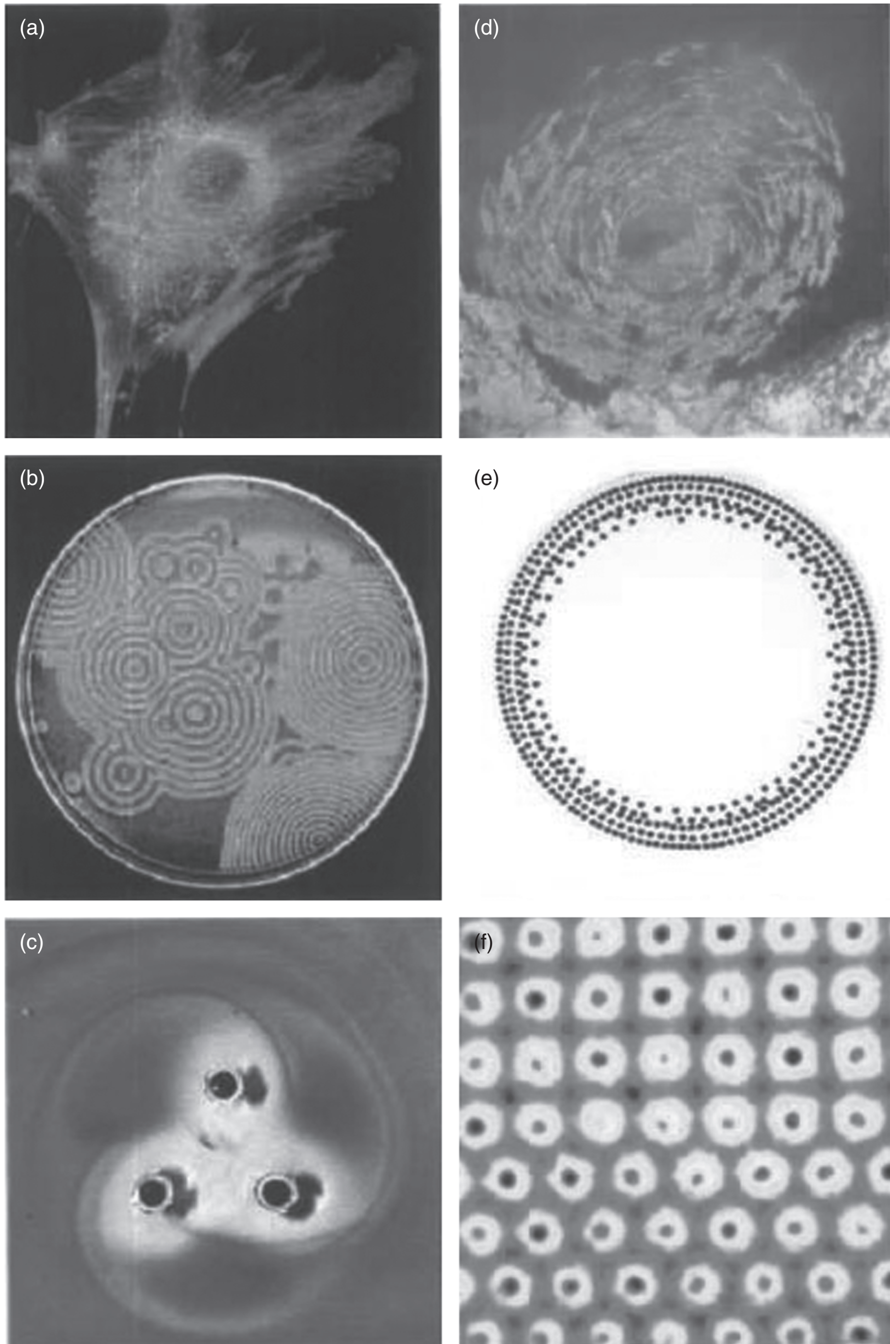

Figure 12.15. Examples of dynamic self-assembly: (A) an optical micrograph of a cell [204], (B) reaction–diffusion waves in Belousov–Zabatinski reaction [61], (C) a simple aggregate of a magnetized disk [205], (D) a school of fish [61], (E) concentric rings by charged metallic beads [61], and (F) convection cells above a metallic support [61].

Templating from Molecules. Some organic nanostructures, which are not totally functional, can be used as templates to mask the deposition of metal or to guide the deposition of metal nanoparticles and nanowires [65, 66]. Patterning block copolymers can be achieved by the combined usage of top-down and bottom-up approaches. Extreme ultraviolet (EUV) interferometric lithography can be used to pattern oxidized SAMs or random copolymers on silica [67]. When a block of copolymer is made to self-assemble, the patterned SAM has the role of a template that guides the phase separation of the polymer. Moreover, regular copolymer structures can also be formed by annealing a block copolymer film confined by physical boundaries [68]. Low level of defects, ability to control and pattern the phase-segregated regions, and controlled drift in the pattern over nonlocal dimensions are the advantages of this approach compared to nontemplated self-assembly.

Templating from Polymers. The modification of colloidal particle surfaces can be realized by using charged polymers and polyelectrodes [69]. Electrostatic attraction between charged surface and charged particles suffices for the adsorption. In most of the cases, polymers have excess charge; therefore, they change/reverse the charge on the surface [70]. This electrostatic change on the surface allows for the formation of another polymer layer, which has the oppositely signed charge of the first polymer layer. As a result, a layer-by-layer assembly process is observed. Colloidal particles are also used to template the self-assembly of nanoparticles that have diameters of >100 nm in general [71].

Templating Using External Forces. Nanospheres with similar sizes and shapes can be employed in the production of thin films of ordered lattices by using their tendency to self-assemble. In order to direct the self-assembly of nanoparticles and nanorods with different structures, electric [72], magnetic [73], shear forces [74], and additional spatial constraints[75] are used. Compared to nanospheres, the self-assembly of nanowires and nanorods is more difficult because these nanostructures have anisotropic forms [76]. Self-assembled nanowires are observed in partially ordered, small domains.

According to another classification of templated self-assembly, there are three main approaches; these are patterned chemical modifications of the surface, patterned charge, and patterned topography [77]. Preferential adsorption of particles on to the selected regions can be observed using the first approach, that is, patterned chemical modifications of the surface of the substrate [78]. The second approach can be realized by using FIB radiation [79], microcontact printing of alkanethiols on gold [80], selective adsorption of polyelectrolytes [81], and electrostatic microcontact printing [82]. Well-ordered high-quality lattices could not be observed using these methods. In order to confine and control colloidal assemblies, patterned topography of the substrate, like wells [83], lithographically patterned reliefs [84], or microfluidic channels[85] are used in the literature. The ratio of the size of the particle to the size of the patterned feature affects the formation of the resulting lattices [86]. Also, shape-selective reliefs, physical boundaries, and external fields are effective on the form of the lattice. An example of such a process is illustrated in Figure 12.16 [77].

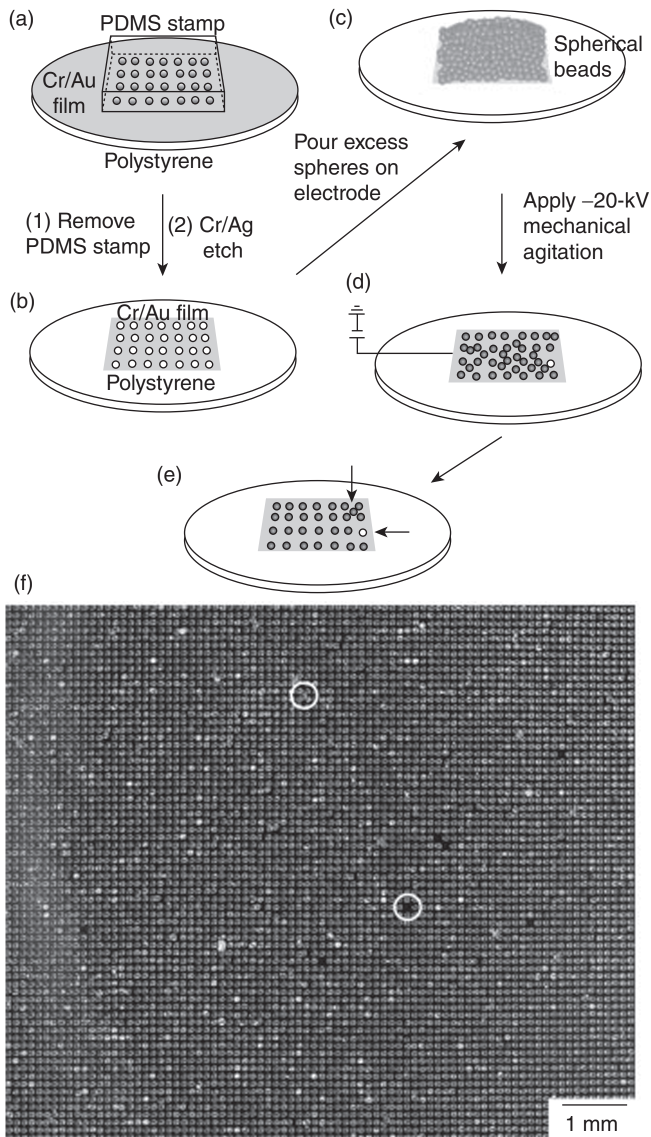

Figure 12.16. Schematic representation of template-directed self-assembly microspheres on a patterned gold electrode using an applied electric field: (a, b) microcontact printing and etching building a templated electrode; (c, d) microspheres self-assembled over the templated electrodes under –20-kV voltage applied to gold electrode; (e) ideally, one microsphere remained on each window and no microspheres on the gold surface; and (f) a typical large-area square matrix of microspheres [77].

Inorganic Templates. Alumina nanoholes and inorganic nanowires are successfully used in the templated self-assembly of nanoparticles [87]. These provide better toughness and prevent changes in the structural characteristics of nanoparticles [88]. Wirelike or rodlike nanostructures are assembled by using alumina nanoholes as templates, which are created by electrochemical etching. Anodic porous aluminas serve as nanocells that are used by building various nanostructured arrays, like magnetic nanorod arrays for longitudinal magnetic data storage, semiconductor particles for optical devices [89], and electroluminescence display devices [90]. These arrays can be used in assembling large-area arrays of parallel wires.

Nanoparticle assembly can be realized both inside and outside these nanowires/rods. As an example, the work of Ajayan and Iijima can be shown, in which they arrange Pd nanoparticles into the carbon nanotubes using capillary forces [91]. Nanoparticles can be assembled outside of these nanotemplates by direct deposition of material (physical or chemical deposition), sol–gel approach, or modifications of the surface functionalities [92].

Biological Templates. Motivation for the use of self-assembly in nanofabrication comes from the observation that many biological structures are assembled by the molecular-level self-assembly [93]. DNA strands [94], peptides [95], and viruses[96] are the possible templates on which a significant amount of research work currently continues. Covalent and noncovalent interactions are in charge during the assembly of nanostructures on these templates. Direct deposition or in situ growth of nanoparticles on these templates can be realized.

Chemically Assisted Assembly

Highly ordered nanoparticle assemblies or patterns can be created using a chemically assisted self-assembly technique [87, 97]. This technique is based on the covalent and noncovalent interactions of a nanoparticle surface protecting group. This approach is widely preferred both in solution and on surfaces. Chemically assisted self-assembly of nanoparticles can be applied by electrostatic layer-by-layer assembly, chemical templating, and SAM methods.

Hydrogen Bonding. Hydrogen bonding is one of the most investigated interaction types for the assembly of nanoparticles together with electrostatic interactions. Based on the hydrogen bonding phenomena, the exchange cross-linking precipitation route for nanoparticle assembly on surfaces is developed. Zirbs et al. showed, for example, the highly selective assembly of barbituric acid-stabilized Au nanoparticles onto Au substrates covered with Hamiltonian-type receptors (Fig. 12.17) [98].

Additionally, different biomolecular linkers are also used for the assembly of nanoparticles based on hydrogen bonding [99]. The chemical characteristics of these molecules are very critical in order to realize the assembly of nanoparticles such as antibody–antigen interactions [100].

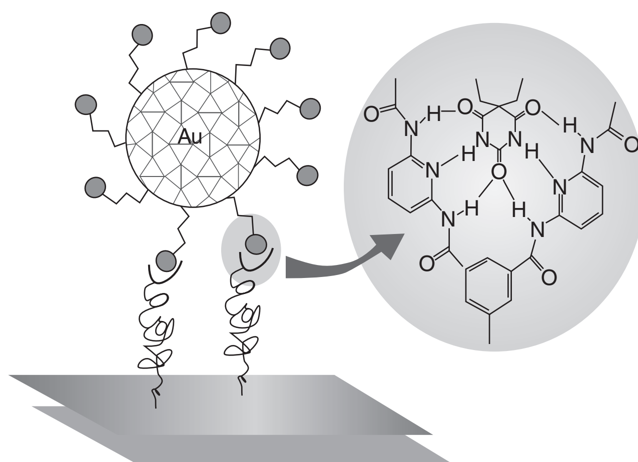

Figure 12.17. Directed self-assembly of Au nanoparticles via multiple hydrogen bonding [98].

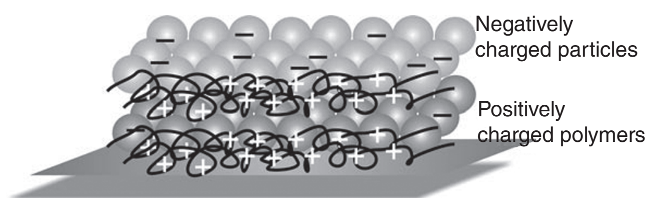

Figure 12.18. Electrostatic assembly of negatively charged particles on positively charged polymers [87].

Electrostatic Assembly. Simple and flexible layer-by-layer assembled nanostructures can be created using electrostatic interactions (Fig. 12.18) [87]. Using this approach, different materials with various optical and electronic properties are structured. The layer-by-layer assembly is first declared by Decher using polyelectroytes [69], whereas Iler reported it for macroscale colloids [101]. However, the use of this technique for nanoparticle assembly is reported by Kotov et al. for the first time [102].

Entropic, van der Waals, steric, dipolar forces and electric charges on the sterically charged nanoparticles are effective in the determination of the stoichiometry of the structures. In general, the nanoparticles are negatively charged, whereas the polymer has a positive charge.

Layer-by-layer assembly is also possible by the epitaxial growth of layers. This technique is especially preferred in the production of different optoelectronic devices, for example, light-emitting diodes. Different layers of thin films are grown epitaxially while using MOCVD. Demir and coworkers hybridized nanocrystals, which are excited by near UV or blue light coming from the diode, on these LEDs to produce white light [72, 103–105]. By using this method, it is possible to precisely control the color of the emitted light on the chromaticity diagram, its correlated color temperature, and its color rendering index.

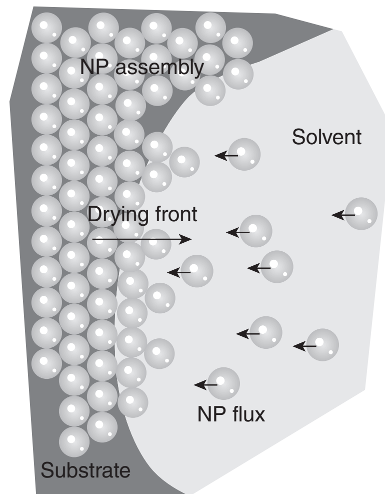

Figure 12.19. Evaporation-induced assembly of nanoparticles (NPs) on surfaces [87].

Drying-Mediated (Evaporation-Induced) Self-Assembly

This method of self-assembly is one of the simplest assembly methods of nanoparticles. Passivated nanoparticles, which are slowly and irreversibly evaporated, assemble in highly ordered patterns on the surfaces (Fig. 12.19) [87]. When the evaporation process is slowed down, the weak attraction forces between nanoparticles in the solution start to be important. According to Denkov et al., the first step of nucleus formation and generation of attractive forces between the particles in the solution results in the second step of the colloidal crystallization [106]. The explanation of the aggregation process is also based on the thermodynamics [107]. The interparticle attractions cannot greatly exceed the thermal energies; therefore, equilibrium structures can be observed depending on the temperature and concentration.

Often the nanoparticles are thought to be uniformly suspended in the solution. The particle concentration increases right underneath of the liquid surface if the diffusion rate of nanoparticles in the liquid is slower than the evaporation speed of the liquid surface. This process often causes the self-assembly of a two-dimensional monolayer at the surface. It is believed that the surface tension is the effective force to hold the assembled structure. Continuation of the evaporation results in the formation of another monolayer on the first layer. If the evaporating region lies on a hydrophilic surface, the dispersed nanoparticles in the solution are positioned toward the drying region by convection. These nanoparticles are dispersed there as the drying front gets thinner.

Continuing the drying process of the nanoparticle solution on surfaces causes the formation of concentric rings with high ordering of quantum dots or other nanoparticles [108]. The rings and the spokes are nanometers in height, submicrons to a few microns in width, and millimeters in length.

Magnetically, Optically, or Electrically Oriented Self-Assembly

The nanoparticles can be aligned and assembled by using magnetic, electric, or optical fields [87]. Electric and magnetic fields lead to the formation of nanoparticle monolayers with increased symmetry [109]. Strong interparticle interactions caused by strong magnetic fields make magnetic nanoparticles assemble in one-, two-, or three-dimensional structures. In general, the ordering of nanoparticles is effected by the external magnetic fields [110]. According to the direction of magnetic field, nanostructures can be grown in a specified direction [111].

Like magnetic fields, electric fields can also be used in the assembly of nanoparticles. In the work of Hermanson et al., micrometer-long wires are created by assembling simple colloidal metallic particles suspended in water under applied electric field [112]. The assembly process relies on the mobility and interactions of particles related to the alternating electric fields (dielectrophoresis [DEP]). In the presence of an alternating electric field, the manipulation and assembly of particles are observed without the interference of the electro-osmotic and electrochemical effects existing in the direct current system. Microwire formation can be described as a collective effect in which the nanoparticles gather at the end of the tip to extend the wire in the direction of the field gradient. The growth of the wire can be effected by controlling the homogeneity of the electric field.

In addition to the magnetic field- and electric field-directed self-assembly, the nanocrystals can also be assembled under the illumination of light [113]. When the surface-bound amino groups are organized to yield thiol ends, the semiconductor and metal nanocrystals can be assembled using light.

Interfacial Self-Assembly

Another method to assemble nanoparticles for large-scale applications is the interfacial assembly (Fig. 12.20) [114]. For example, in Pickering emulsions, large particles of $>1\ \mu$m stabilize emulsions via adsorption on the liquid–liquid interface [115]. In assembling nanoparticles at the fluid interfaces, a similar approach can be used. This process is highly dependent on the temperature fluctuations and interfacial energy. Lin et al. reported that this assembly process is related to the minimization of the Helmholtz free energy [116]. The particles escape as a result of the thermal activation because of the weak energy associated with the placement of nanoparticles.

Nanoparticles can be easily assembled as densely packed, disordered monolayers. The nanoparticle adsorption depends highly on the size of the particles. Nanoparticle surface modifications change the interfacial energy. In general, small particles assemble more weakly on to the interface in comparison with larger particles. Size-dependent particle exchange is also observed, with larger nanoparticles changing places with the smaller ones at a rate related to their adsorption energies [117]. In general, important factors in these processes are the dipole moment, small positive charge, and directional hydrophobic attractions.

In another method, based on hydrophobic interactions, surface-protected nanoparticles are gathered on the water surface. Here, a monolayer formation is observed at

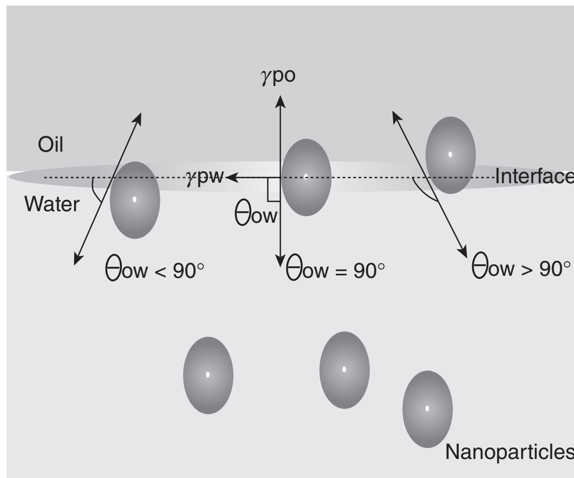

Figure 12.20. Interfacial self-assembly is controlled by the tension of two phases and the contact angle. Energy balance relationship is as follows: $\Delta E = -\pi r^2/\gamma_{OW} \times (\gamma_{OW} - [\gamma_{PW} - \gamma_{PO}])^2$. γ, interfacial energy; P, particle; W, water; O, oil; r, effective NP radius [206].

the water–air interface. Compressing this monolayer slowly, the nanoparticles are transferred to substrates via horizontal or vertical liftoff.

Shape-Selective Assembly

Nonspherical nanoparticles with varying shapes like tetra-/octahedral or cubic can be produced [87]. With these nanoparticles having different shapes, interparticle forces play a critical role in their assembly. As a result of the different polarity between nanoparticles of different shapes, dipole moments are generated. Using this phenomenon, anisotropic structures can be constructed. Utilizing this anisotropy in adsorption and desorption, the assembly of nanoparticles is observed in different dimensions [118]. The driving force of this assembly procedure is the energy difference between crystallographic planes. Since different structures show different affinities toward different inorganic materials, asymmetric self-assembly of nanoparticles can be achieved. More complex structures can be created by mixing the nanoparticles with different phases and sizes [119]. As a result of the mixture of the solutions of differently sized nanoparticles, phase separation is also observed.

Preparation of nanostructures in controlled arrays requires an understanding of the mechanism of the assembly. After understanding the mechanism, new models need to be found in order to understand possible behaviors of the system according to the changes in the parameters of the system. The hierarchical self-assembly of nanoparticles model, developed by Banin and coworkers, is one of the models that provide understanding on the nanostructure construction [120–122]. This model is based on stochastic calculations that simulate the position changes of self-assembling nanoparticles.

SAMS

SAMs are themselves nanoscale structures that provide some useful controllable properties [123]. Their building process relies on the free energy change of the materials. Metal and metal oxide surfaces have the tendency to adsorb organic materials since the free energy between the surface and ambient environment decreases as a result of this adsorption process [124]. The adsorbed materials may change the stability of the nanostructures on the surface; additionally, they may serve as physical or electrostatic barriers to avoid aggregation.

SAMs are organic structures that are built by the adsorption of molecules from the solution or gas phase onto the solid or liquid surfaces. After adsorption, crystalline and semicrystalline structures can be observed on the surface. Molecules or ligands forming SAMs have head groups that have a strong affinity for a specific substrate. SAMs typically have a thickness of about 1–3 nm [123]. SAMs can be laterally patterned with 10- to 100-nm dimensions while using most of the conventional nanofabrication tools and methods. SAMs have numerous advantages in nanotechnology, some of which are the following: (1) The preparation of SAMs is easy; there is no need for special environments or techniques; (2) SAMs can be built up on objects independent of their size and can be used to alter the chemical and/or physical functionalities of these objects; (3) SAMs can affect the electric and optical properties of metallic structures in relation with the external environment; and (4) SAMs make connections between molecular-level structures and macroscopic interfacial phenomena, like wetting and friction.

SAM Substrate Types

A substrate is defined here as the physical object supporting the surface on which the SAM is to be built. Substrates can be in the form of planar surfaces or even nanostructures that are highly curved. The type of the SAM (and thus its preparation method) is application specific [123]. For example, polycrystalline materials can be used in applications including etch resists, in templates for crystallization, and in model surfaces for biological studies. In order to measure electron transport through organic molecules, single crystals or polycrystalline materials are preferred.

Thin films of metals supported on silicon wafers, glass, mica, or plastic substrates are the most frequently used planar substrates for SAMs. Gold, silver, copper, palladium, platinum, nickel, and their alloys are the materials with which thin films can be conveniently constructed easily using PVD methods.

Among these materials, gold is the most frequently used one since gold can form very good SAMs and it is a well-known material [123]. Additionally, Au can be obtained easily in the form of thin film and colloid. Another advantage of Au is its appropriateness for lithographic processes, although it is an expensive material. Its low affinity for oxidation under melting temperature makes gold favorable for nanofabrication procedures as well.

Thin Films on Glass or Silicon by PVD. A thin primer or adhesion layer of titanium, chromium, or nickel (1–5 nm) and a layer of noble metal (10–200 nm) are the

building blocks of a thin film deposited onto a silicon wafer or glass support [123]. The primer serves as the improvement layer for the adhesion of metals that do not form oxides on substrates with an oxidized surface.

Metals with high melting points form smaller grains than metals with lower melting points. The size differences of the grains affect the properties of the resulting SAMs, which determine their applications. Polycrystalline films with smallest possible grains are used in microcontact printing and etching, whereas films with larger grain sizes are used as an insulation barrier against electrochemical processes or biased electron transport.

Thin Films on Mica. The films are usually produced by thermally evaporating gold at a rate of ~0.1–0.2 nm/s on to a heated (400–650°C) sample of mica. By using this method, thin films with grain sizes of ~1000 nm with flat terraces of ~100 nm in width can be constructed. Using the template stripping method, it is possible to build surfaces with a roughness of <1 nm [125]. This technique is based on gluing a glass slide (or another substrate) onto the gold film that is deposited on mica. Finally, the gold film is removed from the mica to expose the surface initially in direct contact with mica.

Electroless Deposition of Thin Films. Electroless deposition is defined as the process in which chemical reduction of metal salts is used [126]. The advantages of this approach are that it does not require vacuum processing devices, that commercially available chemicals are used in the process, and that there is no need of conductive electrodes in this technique. Therefore, deposition of films onto the nonconducting films can be realized. The electroless methods can be used only with solutions. This is advantageous for the thin-film deposition of nanostructures, including colloids and nanopores.

Underpotential Deposition. For the modification of thin-film surfaces, the underpotential deposition technique is used. This is an electrochemical approach to form a submonolayer coverage of one metal onto another one. This layer grows epitaxially by adopting the ordering of the undersurface [127]. This metal layer varies the physical and optical properties of a SAM.

Mechanisms of Assembly from Gas and Solution

In order to control the assembly process of SAMs, the mechanisms of the assembly should be understood. These processes basically depend on kinetic and thermodynamic factors [123]. For example, for thiolates, though the mechanisms cannot be understood completely, it is certain that the SAM formation is strongly related to the energetics of the metal–sulfur bonds and noncovalent lateral interactions of organic groups. Maximization the attractive lateral forces (van der Waals, hydrogen bonding) results with the assembly of the organic layer.

Organization of SAM thiolates on gold from the gas phase involves complex growth kinetics related to the intermediacy of low-coverage phases. During the SAM

assembly of alkanethiols on gold from the gas phase, it is being thought that a precursor occurs, which may involve chemisorbed thiolates with noncrystalline geometry.

Since the solution environment is relatively complex, the mechanisms of SAM configuration could not be understood in details. It is believed that the assembly from solution obeys a kinetic model like the Langmuir adsorption model [128, 129]. Although it is believed that the evolution pathway of the assembly process in solution is similar to the process in gaseous phase, it could not be demonstrated perfectly.

Patterning of SAMs

There are numerous ways of patterning SAMs, including e-beam and X-ray lithography, atomic beam lithography, patterning by gradient formation, ink-jet printing, and orthogonal self-assembly.

Photolithography. When the SAMs of alkanethiols are exposed to UV light using a pattern of apertures, for example, in a chromium film, the photooxidation process of SAMs can be observed in the UV light-illuminated regions [130]. The species, which are photooxidized, can be removed from the substrate using a polar solvent, for example, water or ethanol, for rinsing operation. The resolution of the procedure and produced structures depends on the capability of the optical devices that are used. For UV exposure, the resolution limit is ~0.3 μm [130], and the minimum required time for the exposure is 15 min. Using a phase mask, arrays of lines with 100 nm in ca. 1 min can be produced [131]. Using laser beams, thermal desorption on the SAM can be realized [132], which can be further used to pattern SAMs. Although its exposure time is as short as 0.1 s, the feature size remains to be as large as 20 μm.

E-Beam and X-Ray Lithography. SAMs can also be patterned by using electron beams [133]. The electrons with low energies cause chemical changes in SAMs such as cleavage of bonds, formation of bonds, cross-linking of adjacent molecules, fragmentation of molecules, and conformational disorder [134]. These chemically changed regions are observed to have better resistance against etchants. By using this property, SAM features can be patterned. As another high-energy radiation source to pattern SAMs, X-rays can be used as well [135]. It is observed that X-rays cause similar chemical changes to electron beams on SAMs [136].

Atomic Beam Lithography. SAM patterning can be realized by using rare gases as well. Neutral rare gases that are excited into metastable states can be used to damage SAMs [137]. As a result of the collision of the metastable atom and SAM, energy is released and the metastable atom returns to its ground state. During this process, organic material is locally ionized [138]; here, conformational disorder is observed [139].

Gradient Formation. In order to produce uniform lateral gradients of SAMs, which consist of one or two molecular components, there are several methods, including (1) controlled immersion of one thiol and subsequent immersion in a second thiol (Fig. 12.21) [140], (2) diffusion of two thiols from opposite ends of a gold substrate [141],

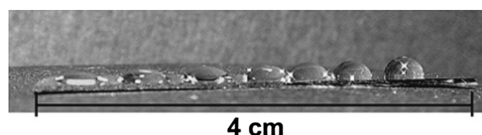

Figure 12.21. Optical photograph demonstrating a gradient in hydrophilicity [140].

(3) electrochemical desorption of thiols from dynamic or potential gradients [142], and (4) gray-scale photolithography on photosensitive SAMs [143].

Ink-Jet Printing. Commercial ink-jet printers are used to deposit nanoliter volumes of solutions with organic dyes onto surfaces like paper. This technology can be used to deposit solutions on metals to construct patterns of SAMs with 100-μm feature size [144].

Orthogonal Self-Assembly. Generation of substrates, which consist of two or more materials, can be considered as an alternative approach for SAM patterning. These generated substrates then form SAMs having affinities toward certain materials.

Current Applications of SAMs in Nanofabrication from Integration Point of View

In the formation of nanoscale features and objects, templated synthesis is a promising approach [123]. Using interesting physical, electrical, and optical properties of these structures, a variety of devices including sensors, selective filters, and probes for biological applications can be designed. Since these structures have smaller sizes in comparison with the cells, a large range of biological applications exists. Alkanethiols can be used to add new functionalities to the SAMs and metals like gold, on which SAMs can form.

In the work of Martin [145], length-controllable nanowires with different metal compositions are demonstrated by using the electrodeposition of metals within mesoporous carbonate or alumina membranes. By using these rods, the orthogonal functionalization of different metallic sections with different SAMs can be realized. Additionally, it is shown that by using charged cysteine SAMs, the ion flux through nanopores can be controlled [146]. By changing the pH of the solution, the membrane permits either cations or anions. It is also possible to make size selection.

Arrays of metallic nanostructures can be used in cellular automata [147], arrays of biomolecules, cell sorting, and information storage. The block copolymer micelle nanolithography technique can be used in the formation of gold nanoparticles in a close-packed hexagonal lattice. The distance between these dots is dependent on the molecular weight and the linear composition of the copolymer [148]. This procedure includes, first, the preparation of a single layer of adsorbed micelles by removing a glass slide from a block copolymer micellar solution, which is also in coordination with Au(III) salt. The self-assembly of micelles is observed in a hexagonal lattice on the surface of the slide. After hydrogen plasma treatment, a hexagonal array of gold

nanoparticles is produced. More complex nanoparticles can be produced using the focused e-beam technique [149].

Colloidal crystals of hexagonal close-packed silica or polystyrene (PS) spheres are used as mask in the nanosphere lithography technique for material deposition [150]. Silver nanoparticle arrays with triangular shape and regular size and spacing can be constructed on various surfaces using this technique.

Metallic half shells are created using e-beam deposition of thin layers of metal onto colloidal arrays. Dissolving colloidal spheres results in free metallic half shells that have nanometer-sized thicknesses.

SAMs can be used to stabilize nanoparticles during their formation. However, a range of functional groups are observed between the nanoparticle and the environment at the interface. Polyvalent interactions of biological tools and platforms are studied by using these functional groups.

ASSEMBLY OF NANOCRYSTALS

Epitaxially Grown, Self-Organized Solid-State Quantum Dots

Two-dimensional planes of semiconductors can be built by using MBE and metal organic vapor-phase epitaxy (MOVPE or MOCVD) methods with nanoscale precision [151]. These techniques can also be applied to assemble quantum dots on semiconductor surfaces by using the principle of lattice mismatch between alternating layers [152]. In this method, a thin layer is epitaxially grown on a substrate with a different lattice constant, such that occurring strain can lead the self-organization of quantum dots. The size and distribution of the quantum dots are dependent on the temperature, substrate angle, flux ratio, lattice mismatch, and growth rate [153, 154].

Self-Assembly of Colloidal Quantum Dots

By setting the surface chemistry of colloidal nanocrystal quantum dots appropriately, ordered self-assembled nanocrystal superlattices in two and three dimensions can be achieved [155].The interactions between these nanocrystals is mostly based on the van der Waals force between them [151].

FePt magnetic nanocrystals can be aligned using the thermal annealing approach. These nanocrystals build up a face-centered tetragonal superlattice. These structures hold promise for data storage applications [156].

The biological systems are also widely investigated for the self-assembly of nanocrystals and nanowires. Gold nanocrystals are assembled using DNA strands [157]. In the mixture of gold nanocrystals and DNA strands, gold nanocrystals form mixtures of dimer (two nanocrystals) and trimer aggregates (three nanocrystals).

Simultaneous reduction of $Pt(acac)_2$ and thermodecomposition of $Co_2(CO)_8$ result in $CoPt_3$ magnetic nanocrystal formation in the presence of organic molecules terminating the growth of Co–Pt bulk phases [158]. Because these nanocrystals have similar sizes and uniform spherical shapes, they can be easily self-organized into two- or three-dimensional superlattices. As a result of slow evaporation, the carrier

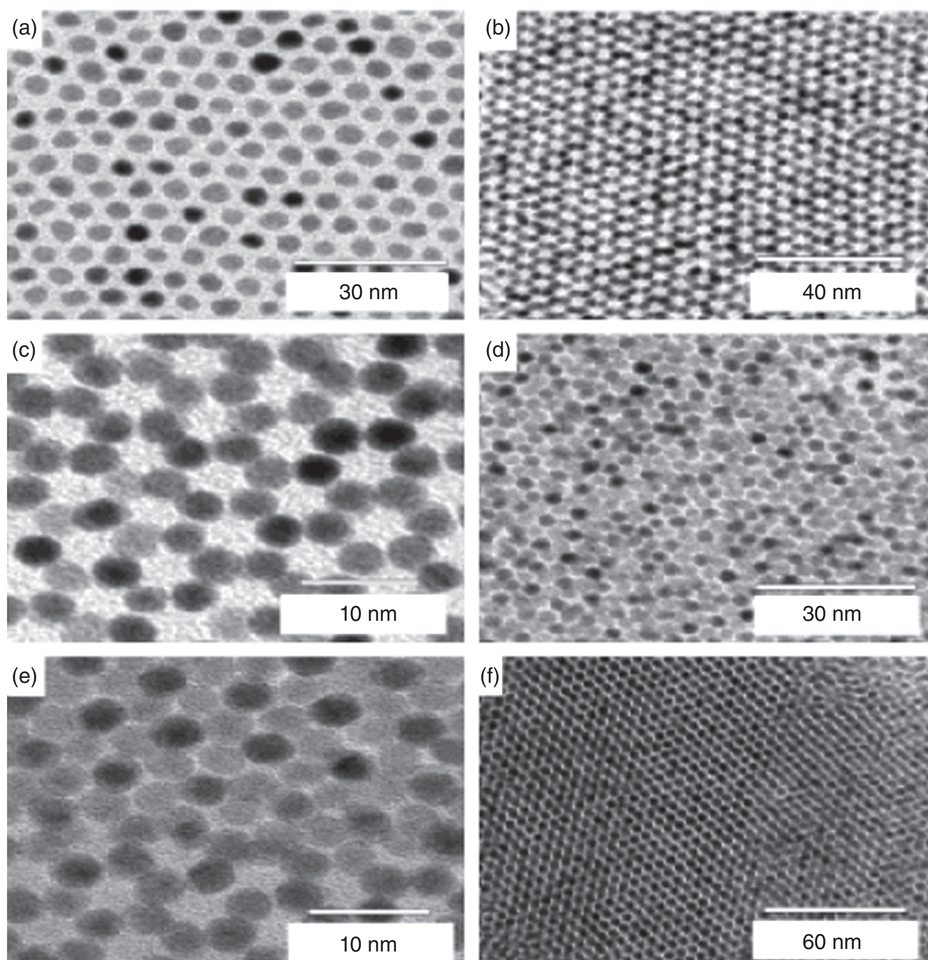

Figure 12.22. TEM images of (a) a 4.8-nm $CoPt_3$ nanoparticle monolayer, (b, c) two layers of 3.6- and 4.0-nm $CoPt_3$ nanoparticles, (d) three layers of 4.0-nm $CoPt_3$ nanoparticles, and (f) more than five layers of 4.5-nm $CoPt_3$ nanoparticles [158].

solvent including colloidal nanocrystals are self-assembled. Several kinds of superstructures are found depending on the solvent evaporation conditions and particle size (Fig. 12.22a).

In case the nanocrystals build more than one monolayer, the nanocrystals in the second monolayer take position between the ones in the first monolayer (Fig. 12.22b, c). The nanocrystals in the third layer are observed to have classical cubic close packing (CCP) (Fig. 12.22d, e).

From monodisperse nanocrystals, the formation of planar superlattices followed [159]. Au or Ag and Au nanoparticles form regular AB_2 and AB alloy superstructures depending on the amount of each species and the ratio of particle diameters.

Nanocrystals that are colloidally synthesized need to be uniform in composition, size, shape, and surface chemistry. The use of thiols as capping agents for II–VI semiconductor nanocrystal synthesis results in molecular-like structures with exact composition [160]. This synthesis operation consists of some consecutive stages: nucleation from initially homogeneous solution, growth of the previously formed nuclei, isolation of particles from the reaction mixture after reaching the desired size, and postpreparative size fractionation.

Nanoparticle Distribution Control by Polymers (According to Aggregation States)

Stabilized Nanoparticles (sNPs) on Microcapsules with Nonuniform Distribution. After the mixture of precoated PS and aqueous suspension of sNPs, they are adsorbed on films due to their positive charge [161]. Using this method, layers from one to six sNP layers are built. This approach makes it possible to adjust the control of the deposited nanoparticle concentration by changing the volume or the concentration of the dipping solution. Although the amount of sNPs can be controlled, the distribution is always observed to be nonuniform.

sNPs on Microcapsules with Uniform Distribution. In the above described method, there is no control over the mechanism of interaction between nanoparticles and the polyelectrolyte surface [161]. The mixture of sNP and identically charged polyelectrolyte leads to a competition between nanoparticles. As a result of this competition, a uniform distribution of nanoparticles is obtained.

Nonstabilized Nanoparticles (nsNPs) on Microcapsules with Nonuniform Distribution. The mixture of precoated PS cores and the suspension of nsNPs result in the adsorption of nanoparticles on films since they are negatively charged [161]. Similar to the sNP case, the amount of nanoparticles can be tuned; however, their distribution becomes nonuniform.

nsNPs on Microcapsules with Uniform Distribution. Premixing the negatively charged nsNP with opposite charged polyelectrolytes forms stable suspensions [161]. It is observed that the polyelectrolytes stabilize the nanoparticles and push them apart upon the adsorption. The result is nonaggregated, uniform distributions of nsNP on the capsules.

Two- and Three-Dimensional Arrays of Monodisperse Nanocrystals Formed by Self-Assembly

The self-assembly process relies on the process of spontaneous formation of ordered arrays from monodisperse particles [160].This effect is caused by the dispersive attraction of nanoparticles due to van der Waals forces [155, 162]. While placing a drop of colloidal solution of monodisperse nanoparticles on a suitable substrate and permitting slow evaporation, self-assembly of two- and three-dimensional arrays can be observed.

The particle spacing in the arrays can be adjusted using different ligands at the synthesis process or by postpreparative exchange [155].As surface coverage increases, nanocrystals tend to form three-dimensional arrays instead of two-dimensional arrays by getting positioned between the nanoparticles of the layer at the top.

Selectivity in Adsorption of Semiconductor Nanocrystals onto a Self-Organized Pattern

Selectivity in the adsorption of semiconductor nanocrystals onto an organic self-organized pattern has a time-dependent behavior [163]. Construction of potential energy landscape on the surface helps to understand the behavior of the delivered solvent. There are two consecutive stages during the self-assembly of patterns: (1) the molecular exchange delivered solvent and lipid molecules to construct the adsorption sites for nanocrystals and (2) the adsorption of nanocrystals onto the adsorption sites because of the interaction between the nanocrystals and the substrate.

Rogach et al. studied the time dependence of nanocrystal deposition controllability [163]. In their experiment, CdSe nanocrystals were dripped in 1-phenyloctane on a patterned surface. After some time, the droplet was taken out using a pipet or a filter paper. This procedure was applied for several different time intervals. If the wetting time remained less than 10 min, the majority of the nanocrystals tended to position in the channels of the patterned surface (Fig. 12.23a). Increasing the waiting/wetting time to 20 min caused the nanocrystals not just to fill in the channels of the patterned surface but also to assemble on the stripes (Fig. 12.23b). Increasing the wetting time even further led to more nanocrystals accumulating on top of the stripes. In Figure 12.23c, a schematic illustration is given for the time dependence of the nanocrystal deposition on wetting time.

In this procedure, the solvent should be carefully selected. The solvent should be chosen to be appropriate for the nanocrystal dispersion, while the selected solvent should not dissolve the selected patterned surface. The surface coverage is modeled by

$$C = -A \cdot \exp(-t/\tau) + \mathrm{C}_0,$$

where C is the surface coverage, A is the front factor, τ is the lifetime, and C_0 is the surface coverage at infinity. The rate constants are different for the different regions of patterned surface.

Au Nanocrystal/DNA Conjugates

There are a variety of biological polymers that can be used to couple nanocrystals. Among these biological structures, DNA is particularly investigated because of its inherent programmability [164]. The Watson–Crick base pairing of an olgionucleotide with 12 bases is thermally stable at room temperature. Twelve base pairs correspond to a length of approximately 4 nm, which contain a sufficient number of pairs for the placement of nanoparticles.

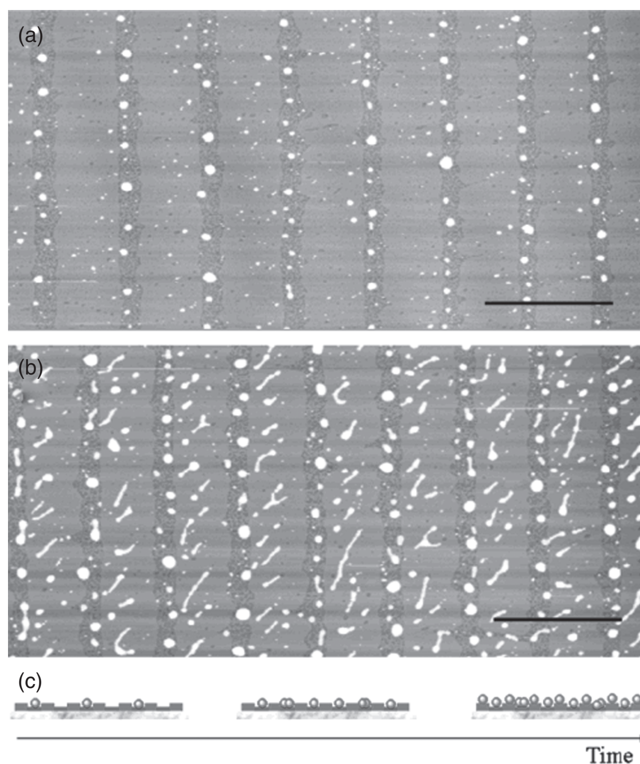

Figure 12.23. AFM images of CdSe nanocrystals on the self-organized lipid patterns show the distribution of nanocrystals with (a) 5-min wetting time and (b) 20-min wetting time. (c) A representative schematic illustration of CdSe nanocrystals depending on wetting time [163].

In order to make use of these properties of DNA/nanocrystal conjugates, it is necessary to have control over the number of nanocrystals conjugating with DNA. Although there is no complete control over this issue, statistical conjugation results are obtained. The average number of DNA strands per particle can be controlled by the adjustment of the DNA:Au ratio.

Entrapment of Nanocrystals in Sol–Gel-Derived Composite Hydrophobic Silica Spheres

An example for the entrapment procedure is given as follows [165]. First, two solutions are prepared. One of the solutions consists of ethanol, ammonium hydroxide, and surfactant Tween 80. The second solution is prepared using tetraethyl orthosilicate (TEOS), various amounts of PS, and toluene solution of the coated nanocrystals. Following the addition of the hydrophobic solution to the hydrophilic solution, the system is stirred overnight. The formed spheres are taken out from the solvent following the centrifugation. The aggregate particles are separated by sonification. Various conditions for specific cases are summarized in Table 12.1.

TABLE 12.1. Entrapment Conditions for Various Nanocrystals in Silica/Polystyrene Spheres [165]

Nanocrystal type and size (nm)	NC amt (mg)	PS amt (mg)	Size of spheres(nm)
CdSe rods, 24.5 × 4.9	20	30	250
CdSe dots, 3.5	40	40	500
CdSe dots, 6.0	20	50	780
CdSe rods, 11.0 × 3.0	30	60	1000
CdSe rods, 15.0 × 3.8	35	30	300
PbSe dots, 10.0	50	40	500
InAs/ZnSe CS, 4.3	20	35	400
InAs/ZnSe CS, 6.3	20	35	400
Au dots, 6.0	30	45	750

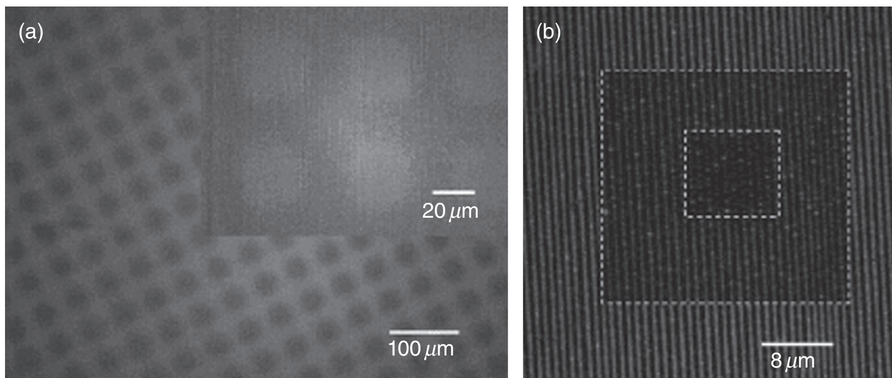

Figure 12.24. Hierarchical luminescence patterns: (a) fluorescence image and (b) confocal laser scanning microscopy (CLSM) image [166].

Hierarchical Luminescence Patterning by Multiscaled Self-Assembly

An alternative method for the nanofabrication hierarchical luminescence patterning is proposed by Chen et al. [166]. Instead of e-beam lithography (EBL) and photolithography, this method offers a self-assembly solution to the nanofabrication. This method involves first generation of two levels of hierarchical luminescence patterning. In the third stage of the process, light is exposed to the samples using a shadow mask (Fig. 12.24a, b).

This approach for nanofabrication offers a relatively inexpensive process; it is also highly controllable, high yielding, and easy to implement. This method also offers the ability to adjust the overall spectrum.

Advantages of Hybrid Nanocomposite Materials with Organic and Inorganic Components

Nanocomposite materials can be classified into two groups [167]: The first class is the inorganic material-embedded polymeric matrix [168], whereas the second class is the organic polymer-embedded inorganic templates [169]. In these approaches, the useful properties of organic components such as good process ability and low density of the polymeric component are combined with the useful properties of inorganic materials, such as their high mechanical durability and well-defined optoelectronic properties.

ALIGNMENT OF NANORODS USING DC ELECTRIC FIELD

Nanostructures including nanorods and nanowires that have significantly different lengths in different dimensions have attracted a great level of attention in scientific research [170, 171]. These structures have the potential to be the fundamental parts of new-generation optical, electrical, and optoelectronic devices [172].

One of the techniques for nanowire production is template-directed assembly. As templates the linear pores and channels in porous materials are used as templates [170]. In the work of Hornyak et al., the production of gold nanowires is reported, while the gold nanocrystals are directed into the pores of an alumina or polymer membrane [173]. Nanowire production also followed using block copolymers as templates [174]. Additionally, further research continues on the production of nanowire by using DNA [175] and viruses [176] as templates. As another template-directed approach, patterned substrates can also be employed in nanowire production. As Yin and Xia [177], and Zhang et al. [178] demonstrated, nanowire production can be realized by a catalyst-mediated phase separation approach [179] and seed-mediated growth in solution [180]. Pacholski et al. successfully demonstrated the production of nanowires by the self-assembly of nanocrystals [181]. In another method, it is proposed to form nanowires from Ag nanocrystal (NC) suspension at the air–water interface and DEP. Moreover, nanowires with different shapes (e.g., linear, zigzag, helical, centipedes, and rings) are produced by the attachment of nanocrystals in different orientations [182]. In addition, micrometer-long nanowires are formed while using the dipole–dipole interactions between spherical nanocrystals [183]. Finally, Rakovich et al. reported the self-assembly of nanocrystals into nanowire networks in phosphate-buffered aqueous solutions [170].

Nanorod Alignment

The deposition of the nanorods from the solution results in an isotropic spatial distribution of nanostructures [184]. However, this situation is not desirable for many applications because the nanostructures are often desired to have shape- and size-dependent optical, electrical, and physical properties. On the other hand, slow evaporation of nanorods from solution leads to slightly ordered structures. This orientation occurs in

the liquid crystalline phase. In this phase, the use of electric field can work for the alignment of nanorods as well.

Electric Field Assembly of Perpendicularly Oriented Nanorod Superlattices

In the work of Ryan et al., perpendicularly oriented II–IV semiconductor nanorod superlattices are formed using DC electric field and slow evaporation of solvent [185]. In this work, CdS nanorods are generated by sulfur/tri-n-octylphosphine solution injection at high temperature into hot cadmium oxide/surfactant mixtures [182]. The DC electric field is applied to the CdS nanorods in toluene that are between two electrodes (Fig. 12.25). The strength of the applied electric field is 1 V/μm. Near saturation of the entire assembly in toluene ensures gentle evaporation. As the evaporation continues, the diameter of the droplets gets smaller, resulting from the formation of nanorods into a planar supercrystal. It is observed that the slower the evaporation is, the higher the degree of spatial order of the nanorods is.

In the absence of the electric field, the nanorods in the outer layers tend to align parallel to the surface, whereas the nanorods at the center are observed to align perpendicular to the substrate. When the electric field is applied, the nanorods tend to position perpendicular to the substrate. Since the electric field is responsible for the rotation of nanorods around their axis to align them perpendicular to the substrate, the evaporation process results with two-dimensional arrays of semiconductor nanorods. Figure 12.26a, b shows the alignment of nanorods in the absence of an electric field, while Figure 12.26c shows a transmission electron microscopy (TEM) image of nanorods aligned under an electric field. Figure 12.26d shows the hexagonal nanorod structures; this alignment is observed when the total growth rate is slow. The evaporation process of the solvent yields densely packed nanorods.

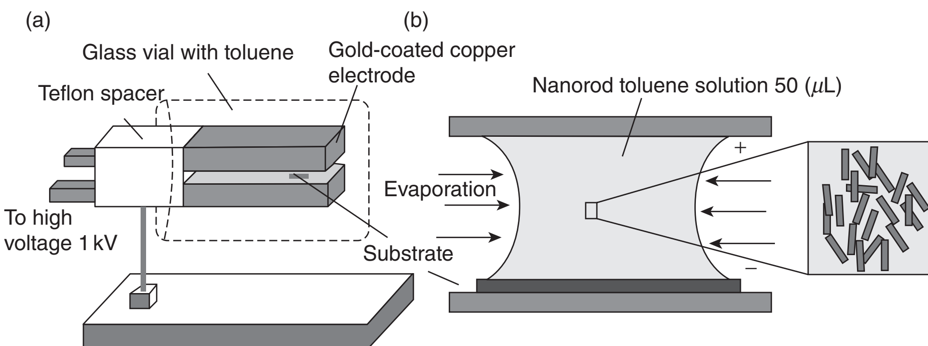

Figure 12.25. Schematic illustration of the electric field assembly of nanorod alignment: (a) a three-dimensional sketch and (b) a two-dimensional view of the meniscus. The substrate is positioned between the electrodes, and 50 μL of the nanorod toluene solution is deposited between the electrodes such that a meniscus is generated [185].

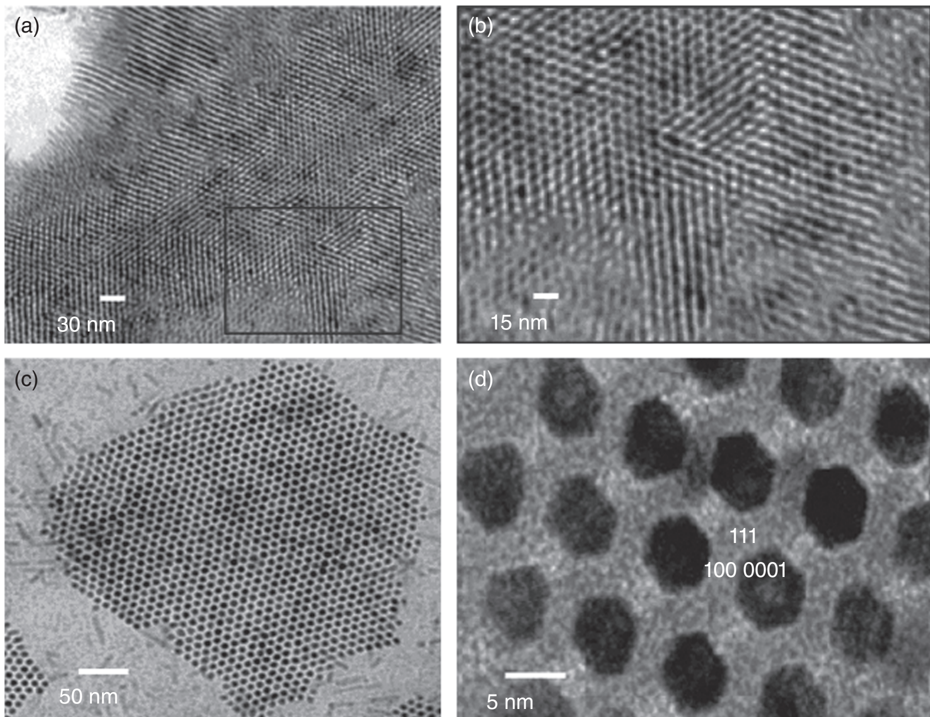

Figure 12.26. (a, b) TEM image of nanorods in the absence of an electric field, (c) TEM image of nanorods aligned under an electric field of 1 V/μm, (d) azimuthal alignment of nanorods [185].

ASSEMBLY OF NANOSTRUCTURES USING DEP AND OPTOELECTRONIC TWEEZERS (OETS)

DEP

To build up devices, high aspect ratio nanostructures, for example, nanowires and nanorods, can be aligned using electric field guiding. By using this method, precise alignment of these nanostructures is achieved across electrodes [186]. Different examples include rod-shaped nanostructures [176, 187] and multiwalled carbon nanotubes [181]. This method provides fast nanowire assembly at room temperature.

The dielectrophoretic forces[188] stem from the induced dipole moment in a non-uniform electric field [189]. This force can be formalized as $\mathbf{f}_{DEP} = (\mathbf{p} \cdot \nabla)\mathbf{E}$, where $\mathbf{p}$ stands for the dipole moment and $\mathbf{E}$ for the electric field. For alternating electric fields, the dielectrophoretic force can be approximated by replacing $\mathbf{p}$ with the effective dipole moment (EDM) of the particle [189]. However, this approximation works only when the particle size is much smaller than the characteristic length of the electric field, which should not be disturbed by the presence of the particle. Therefore, this approximation cannot be used for the objects that are larger than or comparable with the gap between

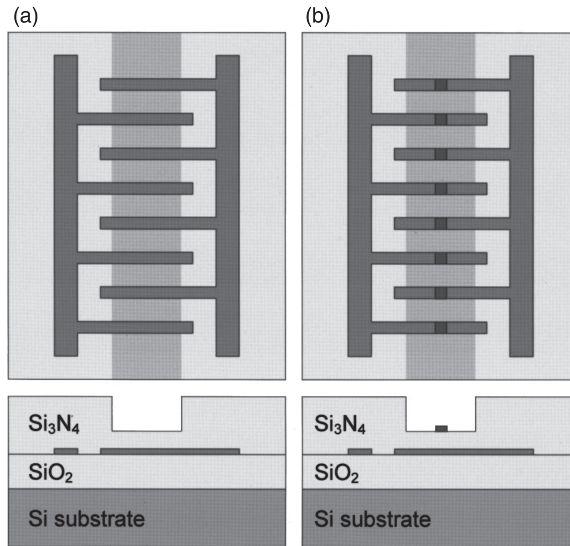

Figure 12.27. Electrode structures used in the electric field guided assembly. (a) Ti/Au electrode with thinned silicon nitride coverage and (b) the same electrode with the addition of top electrodes for the improvement of alignment precision [176].

opposing electrodes. Additionally, it is also problematic when the interaction of multiple particles is considered. To provide a solution for the dielectrophoretic force acting on high aspect ratio nanowires near microelectrodes under electric field, the resulting force and electric field should be computed numerically using the Maxwell stress tensor method [190].

The electric field guided assembly of nanowires in a fluid can be realized using the immersed electrokinetic finite element method (IEFEM). This method involves the movement of independent solid meshes on top of a fixed background fluid using an electric field.

The assembly of nanowires is studied and realized using an electric field by electrically isolated nanowires (Fig. 12.27a) [176]. The metal electrodes are built using 50-nm Ti/150-nm Au liftoff on a silicon dioxide substrate. The finger width and the separation are 3 and 5 μm, respectively. The protection of the electrodes is succeeded by 500 nm of silicon nitride to avoid short circuiting of the electrodes to the metallic nanowires.

The assembly procedure follows: The nanowire suspension is diluted and drop-cast onto the sample, which is biased with AC voltages between $V_{rms} = 5$ V and $V_{rms} = 70$ V. These voltages generate an electric field between 10,000 and 140,000 V/cm given the electrode architecture of the sample. Using this setup, it is observed that the alignment of nanowires is orthogonal to the electrode fingers in the high field regions covered with thin silicon nitride (Fig. 12.28a, b). Another observation is that the alignment occurs if the voltage is greater than $V_{rms} = 25$ V, and nanowire distribution is random. Additionally, it is found out that the relationship between applied voltage and alignment time is inversely proportional.

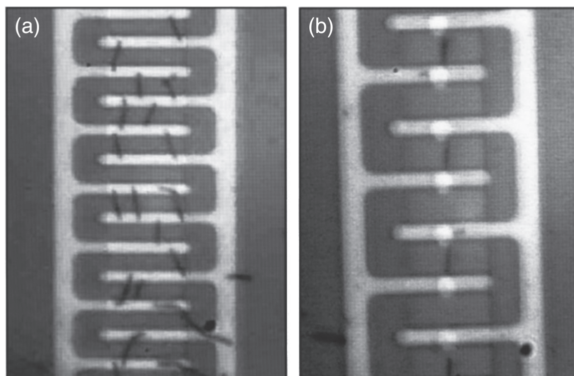

Figure 12.28. Optical microscope image of Au nanowires aligned by the application of (a) 30V at 1kHz with upper field electrodes and (b) 20V at 1kHz with upper field electrodes [176].

It is thought that the random alignment of nanowires is caused by the electric field change between the electrodes following the positioning of a nanowire. The strength of the dielectrophoretic forces is found out to be related to the voltage and time dependencies of the alignment. For low voltages, DEP force remains insufficient, which cannot align the nanowires. Better alignment of nanowires is observed by increasing the applied voltage.

In order to facilitate alignment at certain locations, additional metal electrodes can be deposited on top of the thin silicon nitride layer (Fig. 12.28b). Capacitive coupling between upper and lower electrodes improves the strength of the electric field, which results in better alignment at the periphery of top electrodes.

The frequency dependency of the nanowire alignment process is also investigated. It is found out that the alignment time decreases as the frequency increases. This suggests that the polarization of the dielectric medium around the nanowires is effective in the alignment process at low frequencies. A theory for this phenomenon suggests that at low frequencies, the polar molecules in the dielectric medium can shield the charge separation on the nanowire [191]. However, at high frequencies, the polarized molecules cannot position, such that they shield the charge separation and avoid the torque on the nanowire. Therefore, a strong alignment force can be observed at high frequencies.

The dielectrophoretic force on a spherical particle is given by $\mathbf{F}_{\text{dep}} = 2\pi r^3 \varepsilon_m \text{Re}(K)\nabla \mathbf{E}^2$, where r is the radius of the spherical particle, ε_m is the permittivity of the media, K is the Clausus–Mossotti factor, and E is the electric field. This K factor is a function of permittivity and conductivity of the particle. For the ellipsoid objects with radius r and length l, the complex particle permittivity ε_p^* and medium permittivity ε_m^*, the dielectrophoretic force is given as follows [189]:

$$F_{\text{DEP}} = \frac{\pi r^2 l}{3} \varepsilon_m \,\text{Re}\left\{ \frac{\varepsilon_p^* - \varepsilon_m^*}{\varepsilon_m^*} \right\} \nabla \left| \vec{E} \right|^2 .$$

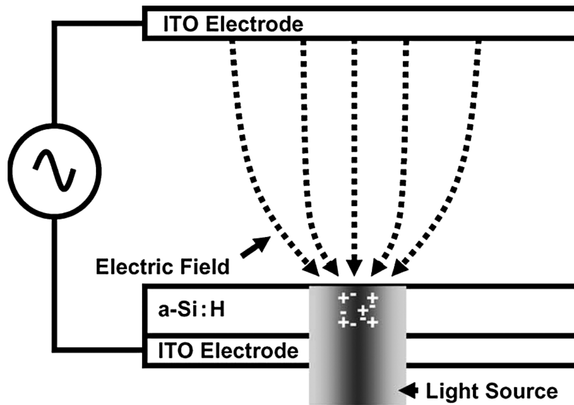

Figure 12.29. Schematics of optoelectronic tweezers [208]. ITO, indium tin oxide.

OETs

The OET method is a combined approach using two different well-known approaches. One approach is the use of optical tweezers to align structures and the other is DEP. The optical tweezer method is developed in the Bell Laboratories by Arthur Ashkin [192]. Using this method, artificial assemblies of cells, colloids, and other objects in three dimensions can be produced by independently controlled tweezers [193]. The main drawback of this method is the weakness of the forces generated by the optical interactions [194]. Increasing the light intensity can be offered as a solution; however, this increase is limited due to the limitations of laser power.

Wu et al. overcome this problem by replacing Ashkin's light forces with dielectrophoretic forces. In the DEP approach, metal electrodes are needed for the establishment of the electric field, which introduces important limitations. Wu et al. removed these limitations by replacing light with electrodes. In other words, optical signals play the role of virtual electrodes formed in a layer of photoconductor (Fig. 12.29) [195].

NANOSKYVING: A NEW METHOD TO PRODUCE ARRAYS OF NANOSTRUCTURES

Nanoskyving uses the deposition of thin films on flat or topographically patterned polymeric substrates using physical vapor methods and subsequent sectioning these films with an ultramicrotome. This technique allows for the fabrication of nanostructures and their arrays for the edges of the thin films [196].

For the nanoskyving method, the first step is to obtain an epoxy substrate after curing an epoxy prepolymer on a flat or topographically patterned PDMS stamp. As the second step, thin films (with nanometer thickness) are deposited onto this epoxy structure. After the generation of the epoxy block containing an embedded thin film,

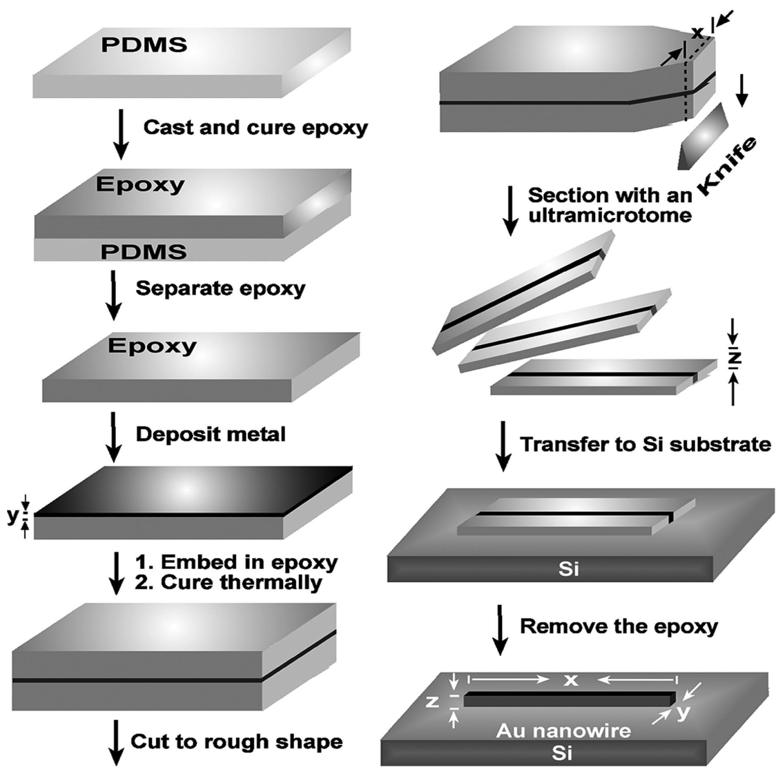

Figure 12.30. Fabrication of metal nanowires as an example of nanoskyving [196].

an ultramicrotome is used to cut this block in slabs that are as thin as 30 nm. After this sectioning operation, the slabs typically float on the surface of water filling the sample collecting reservoir of the microtome (water avoids damage). The removal of epoxy is carried out by oxygen plasma after the epoxy sections are transferred onto a solid substrate (Fig. 12.30).

Nanoskyving builds nanometer-sized structures by cutting thin films deposited on a master structure fabricated in epoxy. Nanoskyving can be thought of as engineering two combined techniques: (1) deposition of the thin film on the master from vapor phase (using e-beam evaporation or sputtering) and (2) sectioning the patterned block by master using a microtome for the production of two-dimensional nanoscale structures. The third dimension is determined by the master topography.

Since the master production is not difficult, nanoskyving does not have an important restriction for the first step in its application. The availability of ultramicrotomes makes nanoskyving implementable for the production of nanostructures that are problematic to produce using conventional techniques such as EUV, X-ray photolithography, EBL, and FIB. In addition, ultramicrotomes are cheaper than clean rooms, e-beam writers, and related equipments [18, 35, 123].

Fabrication of Complex Nanostructures Using Topographically Patterned Substrates

Although Figure 12.30 illustrates a simple structure to fabricate nanosized materials [196], complex nanostructures can also be produced using nanoskyving by choosing the topography of the substrate and selecting the orientation of the sectioning process (Fig. 12.31A). In Figure 12.31B, C, nanostructure arrays with complex patterning are shown as an example.

In nanoskyving, the sliced parts need to be collected before they are transferred onto the substrate layer. Because of its convenience, wet sectioning is the most commonly used sectioning technique. The floating sections/slices are collected and transferred using several techniques. One technique relies on the removal of the slabs using a collection loop, in which a meniscus of water supports the sample. The transfer of the slices can also be achieved by touching the loop to the substrate using the capil-

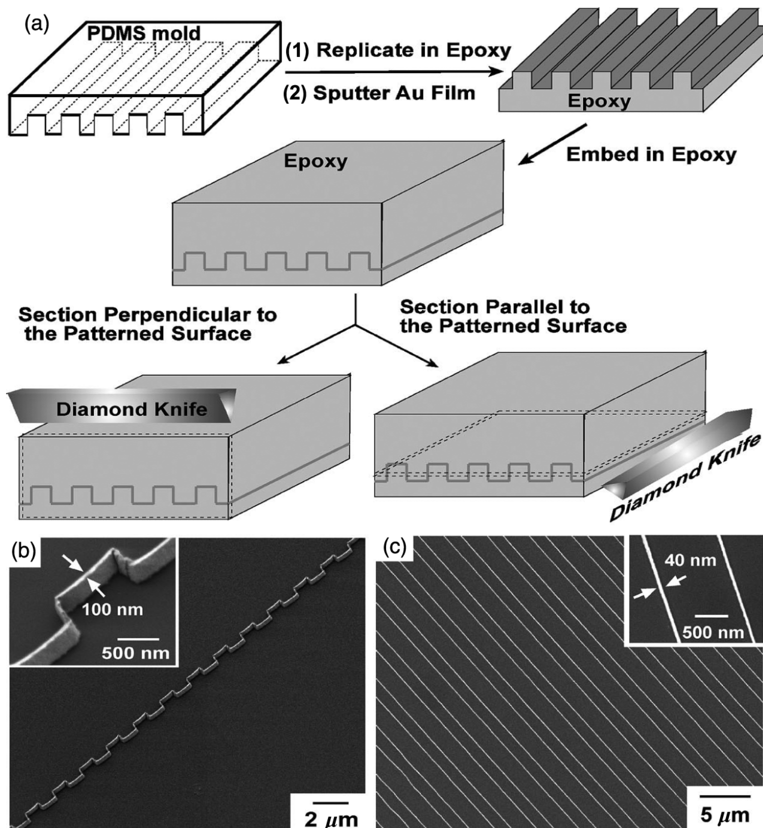

Figure 12.31. (A) Schematic illustration of complex nanostructure production and (B, C) structures obtained by different orientations of slicing, perpendicular and parallel, respectively [196].

lary action. Another method is the collection of slabs by submerging the substrate directly below the floating epoxy slices such that the slices are assembled on the substrate.

Nanoskyving provides simple and inexpensive ways of production of nanostructures in relatively large areas (~mm^2). However, this area still remains small in comparison with the areas patterned by photolithography and nanoimprint lithography, which are on the order of ~500 cm^2 [197]. Nanostructures with higher aspect ratios can be easily produced using nanoskyving, whereas this is a problem in the other methods. Because of the ability to manipulate the slices, the nanomaterials can be easily positioned and assembled on planar or curved regions. In summary, nanoskyving offers substitution of exposure in photolithography, writing in EBL and SPL, and printing/molding in soft and imprint lithography with sectioning by microtome of nanoskyving. However, nanoskyving does not allow the fabrication of connected nanostructures. Therefore, using this technique for integrated circuits seems very difficult. Another drawback of nanoskyving is the lack of stability in the patterns to generate slices that can be registered precisely.

REFERENCES

1. Skogen EJ, Raring JW, Morrison GB, Wang CS, Lal V, Masanovic ML, Coldren LA. 2005. IEEE J Sel Topics Quantum Electron 11:343.
2. Coldren LA, Raring J, Sysak M, Barton J, Johansson L. 2006. Proceedings of Indium Phosphide and Related Materials.
3. Binsma J, Thijs P, VanDongen T, Jansen E, Staring A, Van Den Hoven G, Tiemeijer L. 1997. IEICE Trans Electron E80-C:675.
4. Raring JW, Sysak MN, Tauke-Pedretti A, Dummer M, Skogen EJ, Barton JS, DenBaars SP, Coldren LA. 2006. Proc SPIE 6126:61260H.
5. Aoki M, Suzuki M, Sano H, Kawano T, Ido T, Taniwatari T, Uomi K, Takai A. 1993. IEEE J Quantum Electron 29:2088.
6. Mason B, Fish G, DenBaars S, Coldren L. 1998. IEEE Photon Technol Lett 10:1211.
7. Deppe D, Holonyak N, Jr. 1988. J Appl Phys 64:93.
8. Si SK, Yeo DH, Yoon KH, Kim SJ. 1998. IEEE J Sel Topics Quantum Electron 4:619.
9. Qui B, Bryce A, De La Rue R, Marsh J. 1998. IEEE Photon Technol Lett 10:769.
10. Charbonneau S, Poole P, Feng Y, Aers G, Dion M, Davies M, Goldberg R, Mitchell I. 1995. Appl Phys Lett 67:2954.
11. Skogen EJ, Raring J, Barton J, DenBaars S, Coldren LA. 2003. IEEE J Sel Topics Quantum Electron 9:1183.
12. Skogen EJ, Barton JS, Denbaars SP, Coldren LA. 2002. IEEE J Sel Topics Quantum Electron 8:863–869.
13. Sabnis VA, Demir HV, Fidaner O, Zheng J-F, Harris JS, Jr., Miller DAB, Li N, Wu T-C, Chen H-T, Houng Y-M. 2005. IEEE J Sel Topics Quantum Electron 11:1255.
14. Demir HV, Zheng J-F, Sabnis VA, Fidaner O, Hanberg J, Harris JS Jr., Miller DAB. 2005. IEEE Trans Semiconductor Manufacturing 18:182.
15. So Y-H, Garrou P, Im J-H, Scheck DM. 2001. Chemical Innovation 31:40.

16. Processing procedures for dry-etch cyclotene advanced electronics resins. Dow Chemicals, Tech Rep.
17. Zheng J-F, Demir HV, Sabnis VA, Fidaner O, Harris JS, Jr., Miller DAB. 2006. J Vac Sci Technol B 24:1117.
18. Gates BD, Xu Q, Stewart M, Ryan D, Willson CG, Whitesides GM. 2005. Chem Rev 105:1171.
19. Stewart MD, Patterson K, Somervell MH, Willson CG. 2005. J Phys Org Chem 13:767.
20. Willson CG, Trinque BC. 2003. J Photopolym Sci Technol 16:621.
21. Ito H. 2003. J Polym Sci A 41:3863.
22. http://www.asml.com/asml/show.do?ctx=41905&rid=41906 (accessed May 19, 2011).
23. Switkes M, Kunz RR, Rothschild M, Sinta RF, Yeung M, Baek SY. 2003. J Vac Sci Technol B 21:2794.
24. Bradbury S. 1998. *Introduction to light microscopy*. Oxford, UK: BIOS Scientific Publishers Ltd.
25. Zaidi SH, Brueck SR. 1993. J Vac Sci Technol B 11:658.
26. Bozler CO, Harris CT, Rabe S, Rathman DD, Hollis MA, Smith HI. 1994. J Vac Sci Technol B 12:629.
27. Gamo K. 1996. Microelectron Eng 32:159.
28. Morita T, Kometani R, Watanabe K, Kanda K, Haruyama Y, Hoshino T, Kondo K, Kaito T, Ichihashi T, Fujita J, Ishida M, Ochiai Y, Tajima T, Matsui S. 2003. J Vac Sci Technol B 21:2737.
29. Prewett PD, Gentili M, Maggiora R, Mastrogiacomo L, Watson JG, Turner GS, Brown GW, Plumb D, Leonard Q, Cerrina F. 1992. Microelectron Eng 17:249.
30. Blauner PG, Ro JS, Butt Y, Thompson CV, Melngailis J. 1989. Mater Res Soc Symp Proc 129:483.
31. Kubena RL. 1989. Mater Res Soc Symp Proc 129:483.
32. Ginger DS, Zhang H, Mirkin CA. 2004. Angew Chem Int Ed 43:305.
33. Nyffenegger RM, Penner RM. 1997. Chem Rev 97:1195.
34. Kraemer S, Fuierer RR, Gorman CB. 2003. Chem Rev 103:4367.
35. Gates BD, Xu Q, Love JC, Wolfe DB, Whitesides GM. 2004. Annu Rev Mater Res 34:339.
36. Jung TA, Moser A, Hug HJ, Brodbeck D, Hofer R, Hidber HR, Schwarz UD. 1992. Ultramicroscopy 42:1446.
37. Miyake S, Watanabe S, Miyazawa H, Murakawa M, Kaneko R, Miyamoto T. 1994. Appl Phys Lett 65:3206.
38. Gwo S, Yeh CL, Chen PF, Chou YC, Chen TT. 1999. Appl Phys Lett 74:1090.
39. Vettiger P, Despont M, Drechsler U, Haberle W, Lutwyche MI, Rothuizen HE, Stutz R, Widmer R, Binnig GK. 2000. IBM J Res Dev 44:323.
40. Aizenberg J, Black AJ, Whitesides GM. 1998. Nature 394:868.
41. Pfeiffer L, West KW, Stormer HL, Eisenstein JP, Baldwin KW, Gershoni D, Spector J. 1999. Appl Phys Lett 56:1697.
42. Jun T, Schlitter R, Gimzewski JK, Himpsel FJ. 1995. Appl Phys A 61:467.
43. Himpsel FJ, Jung T, Kirakosian A, Lin JL, Petrovykh DY, Rauscher H, Viernow J. 1999. MRS Bull 24:20.
44. Love JC, Paul KE, Whitesides GM. 2001. Adv Mater 13:604.

45. Yang H, Love JC, Arias F, Whitesides GM. 2002. Chem Mater 14:1385.
46. Melosh NA, Boukai A, Diana F, Gerardot B, Badolato A, Petroff PM, Heath JR. 2003. Science 300:112.
47. Morris RB, Franta DJ, White HS. 1087. J Phys Chem 91:3559.
48. Campbell JK, Sun L, Crooks RM. 1999. J Am Chem Soc 121:3779.
49. Glauert A. 1974. Ultramicroscopy Pt. 2:213.
50. Xu Q, Gates B, Whitesides GM. 2004. J Am Chem Soc 126:1332.
51. Gates B, Xu Q, Thalladi VR, Cao T, Knickerbocker T, Whitesides GM. 2004. Angew Chem Int Ed Engl 43:2780.
52. Haverkorn van Rijsewijk HC, Legierse PEJ, Thomas GE. 1982. Philips Technol Rev 40:287.
53. Colburn M, Johnson S, Stewart M, Damle S, Bailey T, Choi B, Wedlake M, Michaelson T, Sreenivasan SV, Ekerdt JG, Willson CG. 1999. Proc SPIE Int Soc Opt Eng 3676:379.
54. Resnick DJ, Dauksher WJ, Mancini DP, Nordquist KJ, Ainley ES, Gehoski KA, Baker JH, Bailey TC, Choi BJ, Johnson SC, Sreenivasan SV, Ekerdt JG, Willson CG. 2002. Proc SPIE Int Soc Opt Eng 4688:205.
55. Sotomayor Torres CM, Zankovych S, Seekamp J, Kam AP, Cedeno CC, Hoffmann T, Ahopelto J, Reuther F, Pfeiffer K, Bleidiessel G, Gruetzner G, Maximov NV, Heidari B. 2003. Mater Sci Eng 77:596.
56. Zhao XM, Xia Y, Whitesides GM. 1996. Adv Mater 8:837.
57. Kim E, Xia Y, Whitesides GM. 1995. Nature 376:581.
58. Chou SY, Krauss PR, Renstrom PJ. 1995. Appl Phys Lett 67:3114.
59. Chou SY, Krauss PR, Zhang W, Guo L, Zhuang L. 1997. J Vac Sci Technol B 15:2897.
60. Zhao XM, Wilbur JL, Whitesides GM. 1996. Langmuir 12:3257.
61. Whitesides GM, Grzybowski B. 2002. Science 295:2418.
62. Desiraju GR. 1989. *Crystal engineering: the design of organic solids*. Amsterdam: Elsevier.
63. Isaacs L, Chin DN, Bowden N, Xia Y, Whitesides GM, Reinhoudt DN. 1999. In: Reinhoudt DN, ed. *Perspectives in supramolecular chemistry,* New York: VCH, pp. 1–46.
64. Lindsey JS. 1991. New J Chem 15:153.
65. Deng Z, Mao C. 2004. Angew Chem Int Ed 43:4068.
66. Yang J, Mayer M, Kriebel JK, Garstecki P, Whitesides GM. 2004. Angew Chem Int Ed 43:1555.
67. Edwards EW, Montague MF, Solak HH, Hawker CJ, Nealey PF. 2004. Adv Mater 16:1315.
68. Sundrani D, Darling SB, Sibener SJ. 2004. Nano Lett 4:273.
69. Decher G. 1997. Science 277:1232.
70. Afsharrad T, Bailey AI, Luckham PF, Macnaughtan W, Chapman D. 1987. Colloids Surf 25:263.
71. Wang DY, Mohwald HJ. 2004. Mater Chem 14:459.
72. Harnack O, Pacholski C, Weller H, Yasuda A, Wessels JM. 2003. Nano Lett 3:1097.
73. Love JC, Urbach AR, Prentiss MG, Whitesides GM. 2003. J Am Chem Soc 125:12696.
74. Gourdon D, Yasa M, Alig ARG, Li Y, Safinya CR, Israelachvili JN. 2004. Adv Funct Mater 14:238.
75. Nagle L, Ryan D, Cobbe S, Fitzmaurice D. 2003. Nano Lett 3:51.

76. Xia YN, Yang PD, Sun YG, Wu YY, Mayers B, Gates B, Yin YD, Kim F, Yan YQ. 2003. Adv Mater 15:353.
77. Winklemann A, Gates BD, McCarty LS, Whitesides GM. 2005. Adv Mater 17:1507.
78. Fan FQ, Stebe KJ. 2003. Langmuir 19:5179.
79. Fudoizi H, Kobayashi M, Shinya N. 2002. Langmuir 13:7648.
80. Tien J, Terfort A, Whitesides GM. 1997. Langmuir 13:5349.
81. Chen KM, Jiang XP, Kimerling LC, Hammond PT. 2000. Langmuir 16:7825.
82. Jacobs HO, Whitesides GM. 2001. Science 291:1763.
83. Yin YD, Xia YN. 2002. Adv Mater 14:605.
84. Cui Y, Bjork MT, Liddle JA, Sonnichsen C, Boussert B, Alivisatos AP. 2004. Nano Lett 4:1093.
85. Kumacheva E, Garstecki P, Wu HK, Whitesides GM. 2003. Phys Rev Lett 91:128301.
86. Yin YD, Lu Y, Gates B, Xia YN. 2001. J Am Chem Soc 123:8718.
87. Kinge S, Crego-Calama M, Reinhoudt DN. 2008. ChemPhyschem 9:20.
88. Ugarte D, Stoeckli T, Bonard JM, Chatalain A, De Heer WA. 1998. Appl Phys A 67:101.
89. Saito M, Kirihara M, Taniguchi T, Miyagi M. 1989. Appl Phys Lett 55:607.
90. Majetich SA, Yin Y. 1999. Science 284:470.
91. Ajayan PM, Iijima S. 1993. Nature 361:333.
92. Yin LW, Bando Y, Zhu YC, Golberg D, Li MS. 2004. Adv Mater 16:929.
93. Niemeyer CM. 2001. Angew Chem 113:4254.
94. Warner MG, Hutchison JE. 2003. Nat Mater 2:272.
95. Hartgerink JD, Beniash E, Stupp S. 2001. Science 294:1684.
96. Mao C, Solis DJ, Reiss BD, Kottmann ST, Sweeney RY, Hayhurst A, Georgiou G, Iverson B, Belcher AM. 2004. Science 303:213.
97. Chung SW, Ginger DS, Morales MW, Zhang ZF, Chandrasekhar V, Ratner MA, Mirkin CA. 2005. Small 1:64.
98. Zirbs R, Kienberger F, Hinterdorfer P, Binder W. 2005. Langmuir 21:8414.
99. Katz E, Willner I. 2004. Angew Chem 116:6166.
100. Niemeyer C. 2000. Curr Opin Chem Biol 4:609.
101. Iler RK. 1966. J Colloid Interface Sci 21:569.
102. Kotov A, De’ka’ny I, Fendler JH. 1995. J Phys Chem 99:13065.
103. Nizamoglu S, Zengin G, Demir HV. 2008. Appl Physics Lett 92:031102.
104. Huyal IO, Ozel T, Koldemir U, Nizamoglu S, Tuncel D, Demir HV. 2008. Optics Express 16:1115.
105. Demir HV, Nizamoglu S, Ozel T, Mutlugun E, Huyal IO, Sari E, Holder E, Tian N. 2007. New J Phys 9:362.
106. Denkov ND, Velev OD, Kralchevsky PA, Ivanov IB, Yoshimura H, Nagayama K. 1993. Nature 361:26.
107. Gelbart WM, Sear RP, Heath JR, Chaney S. 1999. Faraday Discuss 112:299.
108. Deegan RD, Bakajin O, Dupont TF, Huber G, Nagel SR, Witten TA. 1997. Nature 389:827.
109. Giersig M, Hilgendorff M. 1999. J Phys D 32:L111.
110. Laoste D, TC Lubensky. 2001. Phys Rev E 64:41506.

111. Chushkin Y, Chitu L, Luby S, Majkova E, Satka A, Holy V, Ivan J, Giersig M, Hilgendorff M, Metzger T, Konovalov O. 2005. Mater Res Soc Symp Proc 877E(S6):18.
112. Hermanson KD, Lumsdon SO, Williams JP, Kaler EW, Velev OD. 2001. Science 294:1082.
113. Vossmeyer T, Delonno E, Heath JR. 1997. Angew Chem 109:1123.
114. Binder WH. 2005. Angew Chem 117:5300.
115. Kralchevski PP, Ivanov IB, Ananthapadmanabhan KP, Lips A. 2005. Langmuir 21:50.
116. Lin Y, Skaff H, Ermick T, Dinsmore AD, Russell TP. 2003. Science 299:226.
117. Hamley IW. 2003. Nanotechnology 14:R 39.
118. Tang ZY, Wang Y, Sun K, Kotov NA. 2005. Adv Mater 17:358.
119. Ikkale O, ten Brinke G. 2002. Science 295:2407.
120. Kletenik-Edelman O, Ploshnik E, Salant A, Shenhar R, Banin U, Rabani E. 2008. J Phys Chem C 112:4498.
121. Grousson M, Tarjus G, Viot P. 2000. Phys Rev E 62:7781.
122. TenWolde PR, Sun SX, Chandler D. 2001. Phys Rev E 65:0011201.
123. Love JC, Estroff LA, Kriebel JK, Nuzzo RG, Whitesides GM. 2005. Chem Rev 105:1103.
124. Adamson AW, Gast AP. 1997. *Physical Chemistry of Surfaces*, 6th edition. New York: Wiley-Interscience.
125. Herner M, Wagner P, Semenza G. 1993. Surf Sci 291:39.
126. Baudrand D. 2000. Plat Surf Finish 87:42.
127. Herrero E, Buller LJ, Abruna HD. 2001. Chem Rev 101:1897.
128. Schreiber F. 2000. Prog Surf Sci 65:151.
129. Chen SH, Frank CW. 1990. ACS Symp Serv 447:160.
130. Behm JM, Lykke KR, Pellin MJ, Leggett GJ. 2002. J Am Chem Soc 124:2414.
131. Friebel S, Aizenberg J, Abad S, Wiltzius P. 2000. Appl Phys Lett 77:2406.
132. Shadnam MR, Kirkwood SE, Fedosejevs R, Amirfazli A. 2004. Langmuir 20:2667.
133. Sondag-Huethorst JAM, van Helleputte HRJ, Fokkink LG. 1994. J Appl Phys Lett 64:285.
134. Golzhauser A, Geyer W, Stadler V, Eck W, Grunze M, Edinger K, Weimann T, Hinze PJ. 2000. Vac Sci Technol B 18:3414.
135. Klauser R, Hong IH, Wang SC, Zharnikov M, Paul A, Goelzhaeuser A, Terfort A, Chuang TJ. 2003. J Phys Chem B 107:13133.
136. Heister K, Zharnikov M, Grunze M, Johansson LSO, Ulman A. 2001. Langmuir 17:8.
137. Berggren KK, Bard A, Wilbur JL, Gillaspy JD, Helg AG, McClelland JJ, Rolston SL, Phillips WD, Prentiss M. 1995. Science 269:1255.
138. Harada Y, Masuda S, Ozaki H. 1997. Chem Rev 97:1897.
139. Chabinyc ML, Love JC, Thywissen JH, Cervelli F, Prentiss MG, Whitesides GM. 2003. Langmuir 19:2201.
140. Morgenthaler S, Lee S, Zuercher S, Spencer ND. 2003. Langmuir 19:10459.
141. Liedberg B, Tengvall P. 1995. Langmuir 11:3821.
142. Plummer ST, Bohn PW. 2002. Langmuir 18:4142.
143. Herbert CB, McLernon TL, Hypolite CL, Adams DN, Pikus L, Huang CC, Fields GB, Letourneau PC, Distefano MD, Hu W-S. 1997. Chem Biol 4:731.
144. Bietsch A, Hegner M, Lang HP, Gerber C. 2004. Langmuir 20:5119.
145. Martin CR. 1994. Science 266:1961.

146. Lee SB, Martin CR. 2001. Anal Chem 73:768.
147. Lieberman M, Chellamma S, Varughese B, Wang Y, Lent C, Bernstein GH, Snider G, Peiris FC. 2002. Ann N Y Acad Sci 960:225.
148. Kastle G, Boyen HG, Weigl F, Lengl G, Herzog T, Ziemann P, Riethmuller S, Mayer O, Hartmann C, Spatz JP, Moller M, Ozawa M, Banhart F, Garnier MG, Oelhafen P. 2003. Adv Funct Mater 13:853.
149. Glass R, Arnold M, Blummel J, Kuller A, Moller M, Spatz JP. 2003. Adv Funct Mater 13:569.
150. Haynes CL, Van Duyne RP. 2001. J Phys Chem B 105:5599.
151. Parviz BA, Ryan D, Whitesides GM. 2003. IEEE Trans Adv Packaging 26(3):233–241.
152. Notzel R. 1996. Semicond Sci Technol 11:1365.
153. Solomon GS, Trezza JA, Harris JS. 1995. Appl Phys Lett 66:3161.
154. Solomon GS, Trezza JA, Harris JS. 1995. Appl Phys Lett 66:991.
155. Murray CB, Kagan CR, Bawendi MG. 2000. Annu Rev Mater Sci 30:545.
156. Sun SH, Murray CB, Weller D, Folks L, Moser A. 2000. Science 287:1989.
157. Alivisatos AP, Johnsson KP, Peng XG, TE Wilson, Loweth CJ, Bruchez MP, Schultz PG. 1996. Nature 382:609.
158. Shevchenko EV, Talapin DV, Rogach AL, Kornowski A, Haase M, Weller H. 2002. J Am Chem Soc 124:11480.
159. Kiely CJ, Fink J, Brust M, Bethell D, Schiffrin DJ. 1998. Nature 396:444.
160. Rogach AL, Talapin DV, Shevhenko EV, Kornowski A, Haase M, Weller H. 2002. Adv Fun Mater 12(10):653.
161. Skirtach AG, Dejugnat C, Braun D, Susha AS, Rogach AL, Sukhorukov GB. 2007. J Phys Chem C 111:555.
162. Collier CP, Vossmyer T, Heath JR. 1998. Annu Rev Chem 49:371.
163. Chen X, Hirtz M, Rogach AL, Talapin DV, Fuchs H, Chi L. 2007. Nano Lett 7:3483.
164. Zanchet D, Micheel CM, Parak WJ, Gerion D, Alivisatos AP. 2001. Nano Lett 1:32.
165. Mokari T, Sertchook H, Aharoni A, Ebenstein Y, Avnir D, Banin U. 2005. Chem Mater 17:258.
166. Chen X, Rogach AL, Talapin DV, Fuchs H, Chi L. 2006. J Am Chem Soc 128:9592.
167. Holder E, Tessler N, Rogach AL. 2008. J Mater Chem 18:1064.
168. Gangopadhyay R, De A. 2000. Chem Mater 12:2064.
169. Oriakhi CO. 2000. J Chem Educ 77:1138.
170. Rakovich YP, Volkov Y, Sapra S, Susha AS, Döblinger M, Donegan JF, Rogach AL. 2007. J Phys Chem C 111:18927.
171. Markovich G, Collier CP, Heath JR. 1998. Phys Rev Lett 80:3807.
172. Murray CB, Kagan CR, Bawendi MG. 1995. Science 270:1335.
173. Hornyak GL, Patrissi CJ, Martin CR. 1997. J Phys Chem B 101:1548–1555.
174. Glass R, Arnold M, Blummel J, Kuller A, Moller M, Spatz JP. 2003. Adv. Funct. Mater. 13:569–575.
175. Dujardin E, Hsin L-B, Wang CRC, Mann S. 2001. Chem Commun 1264–1265.
176. Mao C, Christine EF, Hayhurst A, Sweeney R, Qi J, Georgiou G, Iverson B, Belcher AM. 2003. PNAS 100:6947–6951.
177. Yin Y, Xia Y. 2003. J Am Chem Soc 125:2048–2049.

178. Zhang L, Gaponik N, Müller J, Plate U, Weller H, Erker G, Fuchs H, Rogach AL, Chi L. 2005. Small 1:524–527.
179. Hu J, Odom TW, Lieber CM. 1999. Acc Chem Res 32:435–445.
180. Jana NR, Gearheart L, Murphy CJ. 2001. Chem Commun 617.
181. Pacholski C, Karnowski A, Weller H. 2002. Angew Chem Int Ed 41:1188–1191.
182. Cho K-S, Talapin DV, Gaschler W, Murray CB. 2005. J Am Chem Soc 127:7140–7147.
183. Tang Z, Kotov NA, Giersig M. 2002. Science 297:237–240.
184. Scher EC, Manna L, Alivisatos AP. 2003. Phil Trans R Soc Lond A 361:241.
185. Ryan KM, Mastroianni A, Stancil KA, Liu H, Alivisatos AP. 2006. Nano Lett 6:1479.
186. Liu Y, Chung J-H, Liu WK, Ruoff RS. 2006. J Phys Chem B 110:14098.
187. Chen XQ, Saito T, Yamada H, Matsushige K. 2001. Appl Phys Lett 78:3714.
188. Green NG, Morgan H. 2003. *AC Electrokinetics-Colloids and Nanoparticles*. Hertfordshire: Research Studies Press.
189. Jones TB. 1995. *Electromechanics of Particles*. New York: Cambridge University Press.
190. Wang X, Wang XB, Cascoyne PRC. 1997. J Electrost 39:277.
191. Bockris JOM, Reddy AKN. 1970. *Modern electrochemistry*.
192. Ashkin A, Dziedzic JM, Bjorkholm JE, Chu S. 1986. Opt Lett 11:288.
193. Grier DG. 2003. Nature 424:810.
194. Rogers JA. 2008. Nature Photonics 2:69.
195. Chiou PY, Ohta AT, Wu MC. 2005. Nature 436:370.
196. Xu Q, Rioux RM, Dickey MD, Whitesides GM. 2008. Acc Chem Res A41:1566.
197. Li NH, Wu W, Chou SY. 2006. Nano Lett 6:2626.
198. Crommie MF, Lutz CP, Eigler DM. 1993. Science 262:218.
199. Hong S, Zhu J, Mirkin CA. 1999. Science 288:1808.
200. Liu GY, Xu S, Qian Y. 2000. Acc Chem Res 33:457.
201. Ban N, Nissen P, Hansen J, Moore PB, Steitz TA. 2000. Science 289:905.
202. Gracias DH, Kavthekar V, Love JC, Paul KE, Whitesides GM. 2002. Adv Mater 14:235.
203. Clark TD, Tien J, Duffy DC, Paul KE, Whitesides GM. 2001. J Am Chem Soc 123:7677.
204. Whitesides GM, Ismagilov RF. 1999. Science 284:89.
205. Ismagilov RF, Rosmarin D, Gracias DH, Strook AD, Whitesides GM. 2001. Appl Phys Lett 79:439.
206. Zhang H, Edwards EW, Wang D, Möhwald H. 2006. Phys Chem Chem Phys 8:3288.
207. Valley JK, Jamshidi A, Ohta AT, Hsu H-Y, Wu MC. 2008. J Microelectromech Syst 17:342.